Summer 2021

The Role of Symbiotic Algae in the Acclimatization of Oculina arbuscula to Ocean Acidification

Erin M. Arneson

THE ROLE OF SYMBIOTIC ALGAE IN THE ACCLIMATIZATION OF *OCULINA ARBUSCULA* TO OCEAN ACIDIFICATION

by

ERIN ARNESON

(Under the Direction of Daniel Gleason)

ABSTRACT

Ocean acidification (OA) caused by CO_2 emissions is projected to decrease seawater pH to 7.6 by 2100. Scleractinian corals are at risk because excess H^+ in seawater binds to carbonate (CO_3^{2-}), reducing its availability for $CaCO_3$ skeletons. The energy demand for skeletal growth increases as pH decreases because corals must actively purge excess H^+ from their seawater sourced calcifying fluid to maintain high calcification rates. In scleractinian corals it is hypothesized that photosynthesis by symbiotic algae is critical to meet this increased energy demand. To test this hypothesis, I conducted laboratory and field studies with *Oculina arbuscula*, a facultatively symbiotic coral common in the southeastern U.S.A., which exhibits resilience to seasonal fluctuations in pCO_2 that drive pH to as low as 7.8 in the summer. In the lab, aposymbiotic and symbiotic *O. arbuscula* colonies were exposed to a pH of 8.0 or 7.6 for 51 days to test the role of the algal symbiosis in maintaining energy reserves, calcifying fluid pH, skeletal organic matrix and calcification rates during OA. To supplement this controlled laboratory experiment, I transplanted 20 coral colonies to a seafloor CO_2 monitoring platform, exploiting the natural variation in pCO_2 that occurs in Georgia coastal waters. The relationship between calcifying fluid pH and seawater pH was tested for in these samples using boron stable isotopes in coral skeletons. Contrary to the hypothesis, both aposymbiotic and symbiotic *O. arbuscula* colonies maintained similar calcification rates when exposed to OA. Upregulation of calcifying fluid pH, likely fueled by metabolic energy derived from heterotrophy, was the primary acclimatory mechanism detected. Symbiotic algae were associated with higher coral lipid reserves and denser skeletons, but neither of these variables were affected by seawater pH. Corals growing offshore maintained a consistent calcifying fluid pH in the face of seasonal fluctuations in seawater pH and other environmental variables such as temperature and turbidity. The results of my study provide valuable insight into how *O. arbuscula* has evolved to survive harsh

conditions of seasonally low pH levels characteristic of southeastern U.S.A. coastal waters and the mechanisms that may contribute to its future resilience to increasing OA.

INDEX WORDS: Ocean acidification, Temperate coral, Climate change, Carbon dioxide, Coral reefs, Symbioses, Algae, Physiology, Calcification, Calcifying fluid

THE ROLE OF SYMBIOTIC ALGAE IN THE ACCLIMATIZATION OF *OCULINA ARBUSCULA* TO OCEAN ACIDIFICATION

by

ERIN ARNESON

B.S., University of Minnesota, 2016

A Thesis Submitted to the Graduate Faculty of Georgia Southern University in Partial Fulfillment of the

Requirements for the Degree

MASTER OF SCIENCE

COLLEGE OF SCIENCE AND MATHEMATICS

THE ROLE OF SYMBIOTIC ALGAE IN THE ACCLIMATIZATION OF *OCULINA ARBUSCULA* TO OCEAN ACIDIFICATION

by

ERIN ARNESON

Major Professor:	Daniel Gleason
Committee:	John Carroll
	Scott Noakes

Electronic Version Approved:
July 2021

DEDICATION

I would like to dedicate this work to my parents, Ann and Michael Arneson, who unwaveringly fostered in me a love for the outdoors and passion for better stewardship of our earth. Their support in my adventures and unconventional endeavors to follow my dreams has instilled in me the work ethic to complete this degree. I love you both very much!

ACKNOWLEDGMENTS

I would like to acknowledge and thank my academic adviser Dr. Daniel Gleason for mentoring and training me to become a better scientist and for his support in my persistent pursuit of a cross-disciplinary graduate school experience. I want to express my appreciation and thanks to my committee members John Carroll and Scott Noakes for their support and encouragement and for Scott's dedicated ocean acidification monitoring efforts. I am grateful for the hard work of Howie Scher from U of SC, for the weeks spent working out the best methods to help complete the analysis of my isotope samples. Thank you for taking me on as a mentee and for teaching me about boron stable isotopes and ICP-mass spectrometry. I would also like to express my gratitude to the Kemp lab at UAB for welcoming me into their lab and training me on lipid analysis methods. I feel fortunate to have had the help of several undergraduate students. It was a pleasure working with Sarah Rogers, Bailey Yarborough, and Alejandra Daniel. Your support was essential to my lab work. To the staff and my friends at Gray's Reef National Marine Sanctuary, thank you for all the SCUBA diving assistance and moral support. The Dr. Nancy Foster Scholarship Program, the National Marine Sanctuary Staff, and fellow scholars supported and made my last two successful years of graduate school possible. This work was supported in part by an Institutional Grant (NA18OAR4170084) to the Georgia Sea Grant College Program from the National Sea Grant Office, National Oceanic and Atmospheric Administration, US Department of Commerce. *Oculina arbuscula* were collected under the auspices of a letter of acknowledgement from the National Marine Fisheries Service, Southeast Regional Office, St. Petersburg, FL.

Finally, I would like to acknowledge the support from the community of graduate students that I had the pleasure of starting and ending this journey with and am proud to call my Bio Family. And to my entire family, especially my nephews whose infectious enthusiasm for underwater creatures help me stay the course.

TABLE OF CONTENTS

Page

LIST OF TABLES

Page

LIST OF FIGURES

Page

CHAPTER 1

INTRODUCTION

Diffusion of atmospheric carbon dioxide into the ocean, along with intrusion of coastal terrestrial carbon are steadily changing the pH and carbonate chemistry of seawater in a process known as ocean acidification (OA). The numerous chemical changes associated with dissolved organic carbon and atmospheric CO_2 inputs result in the production of carbonic acid (H_2CO_3; equation 1) (Bauer et al. 2013; Noakes 2018).

$$CO_2 + H_2O \leftrightarrow H_2CO_3 \quad (1)$$

The change in pH due to carbonic acid is regulated by the buffering capacity of alkaline molecules in the ocean, such as carbonate (CO_3^{2-}) and borate ($B(OH_4)^-$). As H^+ ions released from the dissociation of carbonic acid (equation 2) are buffered, the concentration of carbonate ions in the ocean is greatly reduced (equation 3. Egleston et al., 2010). This reduction in carbonate ions is one of the greatest concerns regarding OA.

$$H_2CO_3 \leftrightarrow H^+ + HCO_3^- \quad (2)$$

$$CO_2 + H_2O + CO_3^{2-} \leftrightarrow HCO_3^- \quad (3)$$

Carbonate is an essential building block used by many calcifying marine organisms, such as corals, bivalves, and calcifying plankton, to create calcium carbonate ($CaCO_3$) shells and skeletons. Corals have garnered much of the attention within OA organismal research due to their importance as ecosystem engineers (Burke et al. 2011; Huang et al. 2018). Tropical reef systems built by the skeletal structures of coral account for 25% of the ocean's biodiversity. Because corals provide a spatial refuge for many invertebrates and larval fishes in both tropical and temperate systems, OA has the potential for cascading ecosystem level effects (Pörtner 2008; Fabricius et al. 2014; Edmunds et al. 2016).

Seawater pH has declined from 8.2 to 8.1 since the onset of burning fossil fuels during the late 1700s (Orr et al. 2005). Models developed by the Intergovernmental Panel on Climate Change (IPCC) predict a decrease of anywhere from 0.108 to 0.315 for the average open ocean pH by 2100 due to increasing pCO_2 (Bindoff et al. 2019). If seawater pH declines by the latter magnitude, it may cause a

significant decrease in the saturation state of aragonite in many areas of the globe (Doney et al. 2009). Aragonite is the form of $CaCO_3$ present in the majority of scleractinian coral skeletons. As long as the aragonite saturation state of seawater is above 1, the formation of $CaCO_3$ is favored but if it drops below 1, then dissolution of $CaCO_3$ begins. It was initially expected that any reduction in aragonite saturation state would spell disaster for corals by severely impairing their skeletal growth (Marubini et al. 2003; Kroeker et al. 2013). Now decades into OA research, calcification responses appear to vary widely across species (Chan and Connolly 2013; Holcomb et al. 2014; Von Euw et al. 2017; Bove et al. 2019). While the calcification rates of some species are highly sensitive to OA (e.g. *Stylophora pistillata, Psammacora profundacella, Siderastrea radians*), others appear to have coping mechanisms (e.g. *Pocillopora damicornis, Desmophyllum dianthus, Pocillopora acuta*) (Krief et al. 2010; Okazaki et al. 2013; Comeau et al. 2014; Rodolfo-Metalpa et al. 2015; Wall et al. 2017).

The calcification process in corals is driven primarily by biological control of the calcifying fluid and skeletal organic matrix (Cohen and McConnaughey 2003). Calcifying fluid is found in discrete spaces between calicoblastic cells of the ectoderm and the skeletal surface, is only a few nanometers thick, and sourced from seawater (Goldberg 2001). The relative concentrations of dissolved inorganic carbon (CO_3^{2-}, HCO_3^- and CO_2) and pH at the site of calcification are biologically adjusted using carbonic anhydrases, ion and alkalinity pumps (Allemand et al. 1990; Figure 1). Carbonic anhydrases are essential for delivery of inorganic carbon to symbiotic algae within the coral tissue for photosynthesis (Hopkinson et al. 2015). They also play roles in delivering respired CO_2 from the animal to the calcifying fluid and converting it to carbonate (Bertucci et al. 2013). ATP powered ion pumps are responsible for the exchange of $2H^+$ for Ca^{2+} with seawater, which upregulates the internal pH of calcifying fluid (Al-Horani et al. 2003; Venn et al. 2011; Bertucci et al. 2013). Depending on the species, the pH under coral tissue is typically 0.5 to 1 units higher than surrounding seawater and provides one explanation for why corals can continue calcification when seawater chemistry is unfavorable (Raybaud et al. 2017; Lin et al. 2018; Sevilgen et al. 2019). Calcium and CO_2^{2-} sourced from pockets of calcifying fluid nucleate to organic

matrix sites on the existing skeleton. Organic matrix encourages calcification by reducing the free energy needed for nucleation of $CaCO_3$ and acts as a scaffolding, controlling crystal orientation (Cohen and Holcomb 2009; Venn et al. 2011; Drake et al. 2013; Falini et al. 2013). Therefore, organic matrix may provide a second explanation for the maintenance of calcification rates in some species of coral under OA conditions.

Calcification is an energetically costly process, by one estimate requiring up to 30% of a coral's energy budget (Allemand et al. 1990). The ability to compensate for lower seawater aragonite saturation states may depend on the amount of energy a coral is able to allocate to the calcification process. Maintaining sufficient calcifying fluid chemistry alone uses ~1 μmol of ATP for every 1 μmol of $CaCO_3$ produced (McConnaughey and Cohen, 2003). Ocean acidification is expected to increase the ATP required to remove H^+ from calcifying fluid to promote formation of $CaCO_3$. For example, at a pH of 7.6 transcriptome evidence in the Indo-pacific coral *Galaxea fascicularis* points towards upregulation of genes associated with the cellular acid-base homeostasis, exchanging calcium and other ions (Lin et al 2018). The energetic needs for calcification are sourced from the metabolism of macromolecules like carbohydrates, proteins and lipids. Storage, metabolism, and allocation of energetic macromolecules occurs either from the photosynthetic process of algal symbionts present within the endodermal tissue or from heterotrophy by the coral host. Most photosynthetically-derived fixed carbon is translocated and stored in the form of glucose or glycerol, whereas most heterotrophic prey are a richer source of proteins and lipids (Kellogg and Patton 1983; Muscatine et al. 1984). The energetic costs of physiological adjustments to maintain adequate calcification rates are likely to increase with OA stress, making photosynthetic contributions critical for some coral species to overcome calcification challenges.

The differential response of calcification rates to OA is difficult to understand in tropical corals. They all have obligate symbioses, so the response of the algal symbionts versus the coral host to OA can become convoluted. In order to study how OA stress affects carbon flow and allocation of energy, the links between the precipitation of $CaCO_3$ and the photophysiological regime of the endosymbiotic algae

must be decoupled. Temperate and subtropical coral species on the other hand often have a facultative symbiosis with algae and exhibit more resilient responses to OA conditions (Ries et al. 2009; Rodolfo-Metalpa et al. 2010; Griffiths et al. 2019). Exploiting the facultatively symbiotic nature of some of these coral species may facilitate the ability to uncouple the contribution of the host and corresponding algal symbionts in maintaining calcification rates under OA stress.

In tropical corals, energy for skeletal growth is primarily sourced from the symbiotic algae present within the endodermal tissue. Inorganic carbon used by algal symbionts for photosynthesis is derived either from seawater diffusion or the respiration of their coral host. In turn, approximately 95% of the carbon fixed by symbionts gets transferred to the host (Muscatine et al. 1984). It has been hypothesized that OA may enhance the photosynthetic potential of corals due to increased inorganic carbon availability in the surrounding seawater, but few coral species show evidence of this as a mechanism to resist reductions in calcification rates (Langdon and Atkinson 2005). If the ambient seawater pH becomes too low, cellular processes associated with endosymbiotic photosynthesis can be disrupted (Lin et al. 2018). This disruption may occur because DIC normally allocated to photosynthetic algae in tropical corals is instead directed towards the calcifying fluid for conversion into CO_3^{2-} (Lin et al. 2018).

Ocean acidification presents a homeostatic challenge to the coral host. Transcriptome response in *G. fascicularis* suggests the maintenance of homeostasis relies on intracellular energy reserves and the nutritional pool, giving corals the ability to tolerate the external stress (Lin et al. 2018). Considering that energy reserves correlate with survival and recovery from acute stressors like ocean warming (Rodrigues and Grottoli 2006), it is likely that stored lipids and proteins also provide a necessary nutritional pool when OA stress increases energetic demands (Hennige et al. 2014; Maier et al. 2016). Lipid and protein reserves can be accrued from two possible sources, translocated carbon from symbiotic algal photosynthesis or from heterotrophy. Although tropical coral species benefit from the significant contribution of symbiotic algae, they appear to be more sensitive to OA than their aposymbiotic

counterparts in temperate and cold water regions (Rodolfo-Metalpa et al. 2010; McCulloch et al. 2012; Varnerin et al. 2020). Certain species of temperate (*Madrepora oculata)* and cold-water (*Leptopsammia pruvoti)* corals exhibit lipid draw down and maintain typical calcification rates under OA stress in the laboratory (Maier et al. 2016; Movilla et al. 2016). *Desmophyllum dianthus,* also a cold-water coral, has even been shown to tap into less efficient protein catabolism when subjected to the combined stressors of OA and temperature (Gori et al. 2016). This metabolic response suggests heterotrophy is the critical protein and lipid source for maintaining energetic mechanisms needed for processes that drive OA resilience.

If metabolism of energy reserves is indeed one mechanism used by corals for coping with calcification challenges induced by OA, then one would also expect to see correlated control over calcifying fluid chemistry. One method of determining calcifying fluid pH is by using a boron stable isotope proxy. Boron is present in only two forms in seawater, boric acid and borate, which act as important buffers alongside carbonate and bicarbonate. Boron speciates rapidly within the natural pH range of seawater ~7.6-8.2 (Figure 2; equation 4). As seawater pH decreases, the concentration of boric acid increases and borate decreases (equation 4; Hemming and Hanson 1992; Egleston et al., 2010). The boron element also exists in two isotopes, ^{10}B and ^{11}B. The tetrahedral form of borate discriminates against the heavier isotope as a charged and less stable molecule. The stronger bonding environment of the trigonal structured boric acid is therefore enriched with respect to ^{11}B because of its stability. The fractionation factor pertains to the redistribution of isotopes in each compound as their concentrations change in relation to one another. Klochko et al. (2006) experimentally derived this factor to be 1.0272 for boron which is routinely used in foraminifera and coral boron pH proxies to back-calculate pH.

$$B(OH)_4^- + H^+ \leftrightarrow B(OH)_3 + H_2O \qquad (4)$$

The boron pH proxy works because aragonite precipitates selectively with the borate ion in scleractinian coral skeletons so the isotopes measured are related only to the abundance of borate, not boric acid (Noireaux et al. 2015). The isotopic signature of borate included in the skeleton records the pH of the

calcifying fluid at the time of calcification (Trotter et al. 2011; Dissard et al. 2012). When borate concentrations decrease with pH, so does the relative abundance of ^{11}B ($\delta^{11}B$) within the borate molecules. As pH decreases and more boric acid becomes available, there is a redistribution of ^{11}B to the trigonal molecules. To understand this, we can picture what boron would look like at a pH of 6. At a pH below the range of natural seawater, boron would be present primarily as boric acid. In this situation all ^{11}B isotopes would be held by boric acid ($\delta^{11}B_{sw}=\delta^{11}B_{boric\ acid}$).

The two main drivers of calcification in scleractinian corals are calcifying fluid pH and production of organic matrix. Both mechanisms are energetically expensive. Organic matrix reduces the kinetic energy needed for $CaCO_3$ nucleation and controls crystal orientation. It is made up of lipids, carbohydrates, and proteins, comprising between 0.1 and 3% of total skeletal weight (Allemand et al. 2004; Dauphin et al. 2006). Out of the 3 classes of macromolecules present, proteinaceous organic matrix has been observed to exert the most control over the biomineralization process (Weiner and Dove 2003; Adamiano et al. 2014). In *G. fascicularis* and *Stylophora pistilla,* proteinaceous organic matrix production is upregulated in conjunction with exposure to low pH (Tambutté et al. 2015; Lin et al. 2018). Increasing organic matrix has been proposed as another acclimatization response to OA. In fact, as long as the aragonite saturation state of calcifying fluid remains > 1, an increase in organic matrix may be enough to maintain normal calcification rates (Lin et al. 2018). An accurate estimation of the energetic cost to build organic matrix in corals is unknown, so if this is used as a coping mechanism for OA, it may be unsustainable long-term (DeCarlo et al. 2018).

Oculina arbuscula is a branching, facultatively symbiotic coral found along the southeastern coast of the U.S.A. Its range includes the seasonally variable waters of Georgia, where pCO_2 increases during the summer months, reducing seawater pH to as low as 7.8 (Noakes 2018). *Oculina arbuscula* colonizes on hard bottom habitats (Gleason et al. 2018) and is found with or without symbionts of the family Symbiodiniaceae, most commonly *Brevolium psygmophilum* (Thornhill et al. 2008; Leydet and Hellberg 2016; LaJeunesse et al. 2018). Aposymbiotic colonies growing underneath overhangs or on the

vertical sides of ledges are found to reach similar sizes as more exposed symbiotic colonies. In laboratory studies, symbiotic *O. arbuscula* adults and juveniles demonstrated resistance to seawater carbonate chemistry predicted for the end of the century (Ries et al. 2010; Varnerin et al. 2020; Wang et al. 2020). Furthermore, calcification rates only slowed significantly when colonies of *O. arbuscula* were exposed to pCO_2 > 2,800ppm equating to an aragonite saturation state of 0.8 (Ries et al. 2010). The mechanisms behind this resistance to high pCO_2 have not yet been identified. While short term lab experiments suggest *O. arbuscula* will be resilient to future reductions in seawater pH, the health and growth of colonies *in situ* where there are natural fluctuations in pH conditions and other relevant impinging variables such as light and temperature, has yet to be documented.

Employing the facultatively symbiotic nature of *O. arbuscula*, created an opportunity to explore acclimatization mechanisms for corals under increasingly unfavorable seawater carbonate chemistry. Founded on the underlying hypothesis that algal symbionts facilitate the acclimatization of *O. arbuscula* to OA, I predicted the following for aposymbiotic and symbiotic colonies maintained under low pH conditions in the laboratory: 1) energy reserves will remain high in symbiotic colonies and be drawn down in aposymbiotic colonies, 2) the maintenance of a higher energy budget in symbiotic corals due to algal photosynthesis, will be manifested in greater control of calcifying fluid pH and more organic matrix production, and 3) the higher energy reserves and organic matrix production in symbiotic *O. arbuscula* will result in faster calcification rates when compared to their aposymbiotic counterparts (Figure 3). Finally, I incorporated a measure of realism into the laboratory findings by measuring the calcifying fluid chemistry of *O. arbuscula* colonies in a naturally pH variable environment. Based on the results of the laboratory studies I predicted that symbiotic corals offshore would acclimatize to seasonally low seawater pH by upregulating their calcifying fluid pH to a level that allows calcification rates to be maintained.

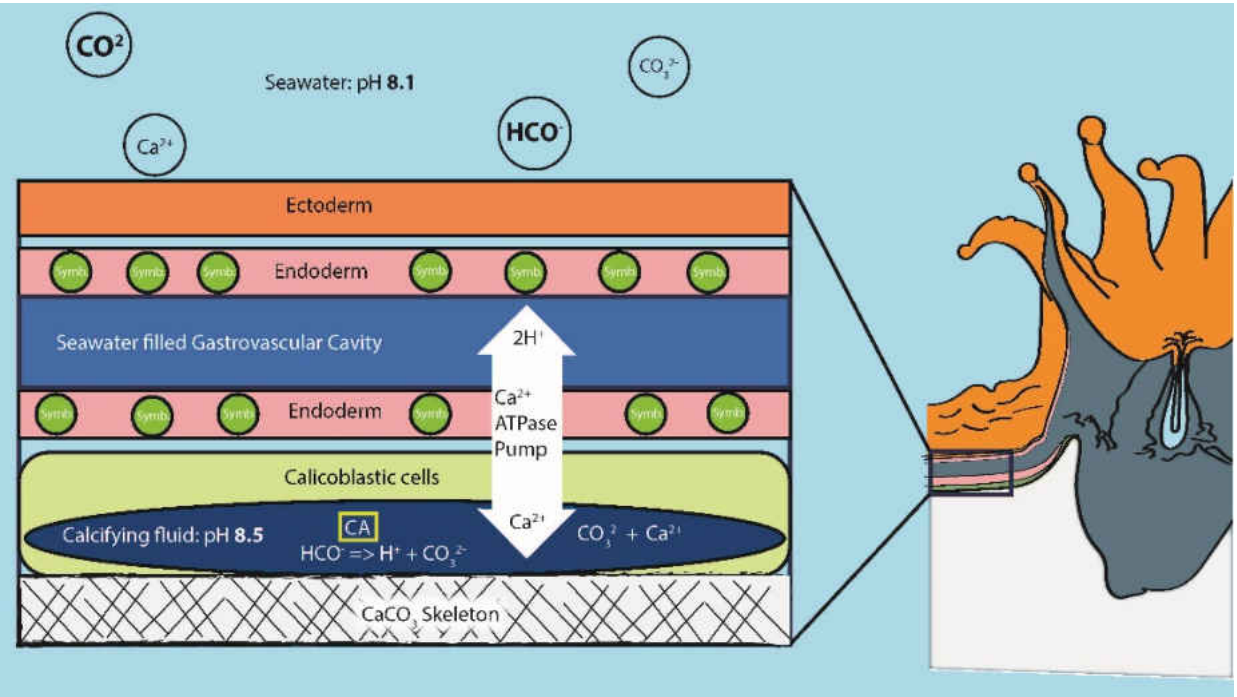

Figure 1. A schematic representation of the calcification process in relation to the ectodermal and endodermal tissue layers of a coral polyp. Photosynthetic symbiotic algae are located within the endoderm encircling the gastrovascular cavity. Calcification takes place between the calicoblastic cells of the endoderm and the existing skeleton. Seawater sourced calcifying fluid is located in this space to provide the skeletal building blocks calcium (Ca^{2+}) and carbonate (CO_3^{2}). The pH of the calcifying fluid is biologically controlled by carbonic anhydrase (CA) enzymes and ATP pumps which actively remove H^{+}. Higher pH levels create favorable environments for calcification with greater concentrations of CO_3^{2-} and Ca^{2+}. The cross hatches within the skeleton represents the organic matrix included in the skeleton which creates scaffolding for $CaCO_3$ nucleation and controls crystal orientation.

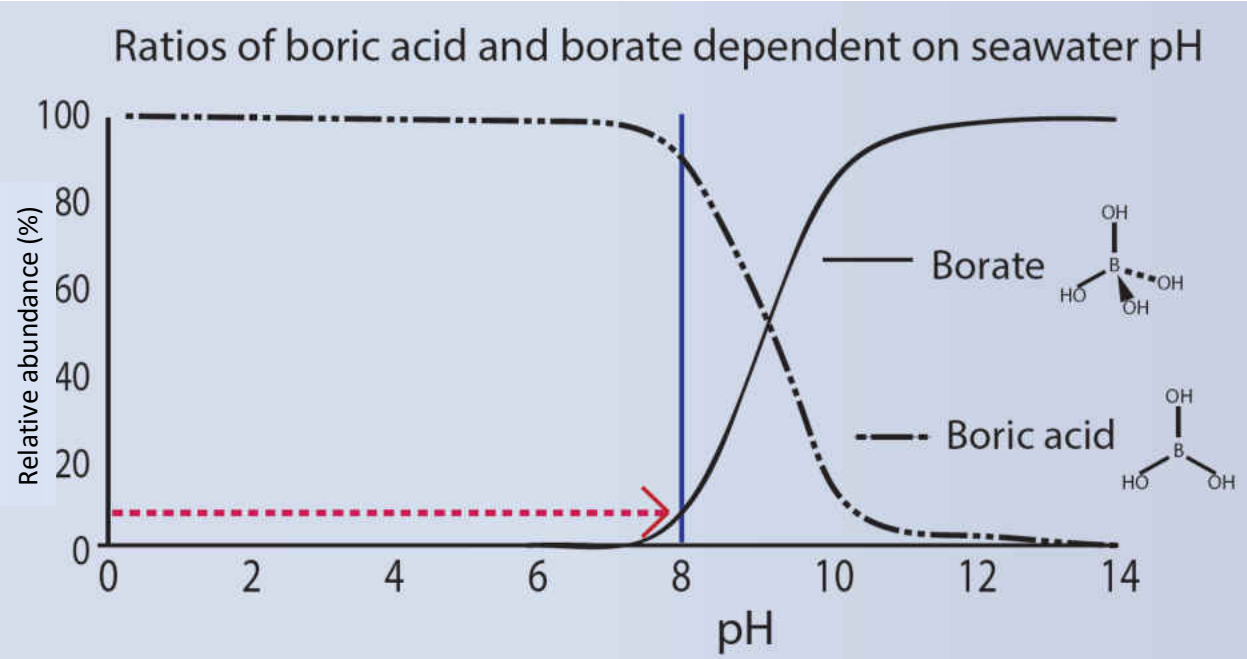

Figure 2. pH dependent equilibrium curves for boric acid and borate in seawater with relative abundance represented as percent of each boron species. The blue line represents the current average seawater pH of 8.1 and the red arrow dentoes the current relative abundance of borate in present day seawater.

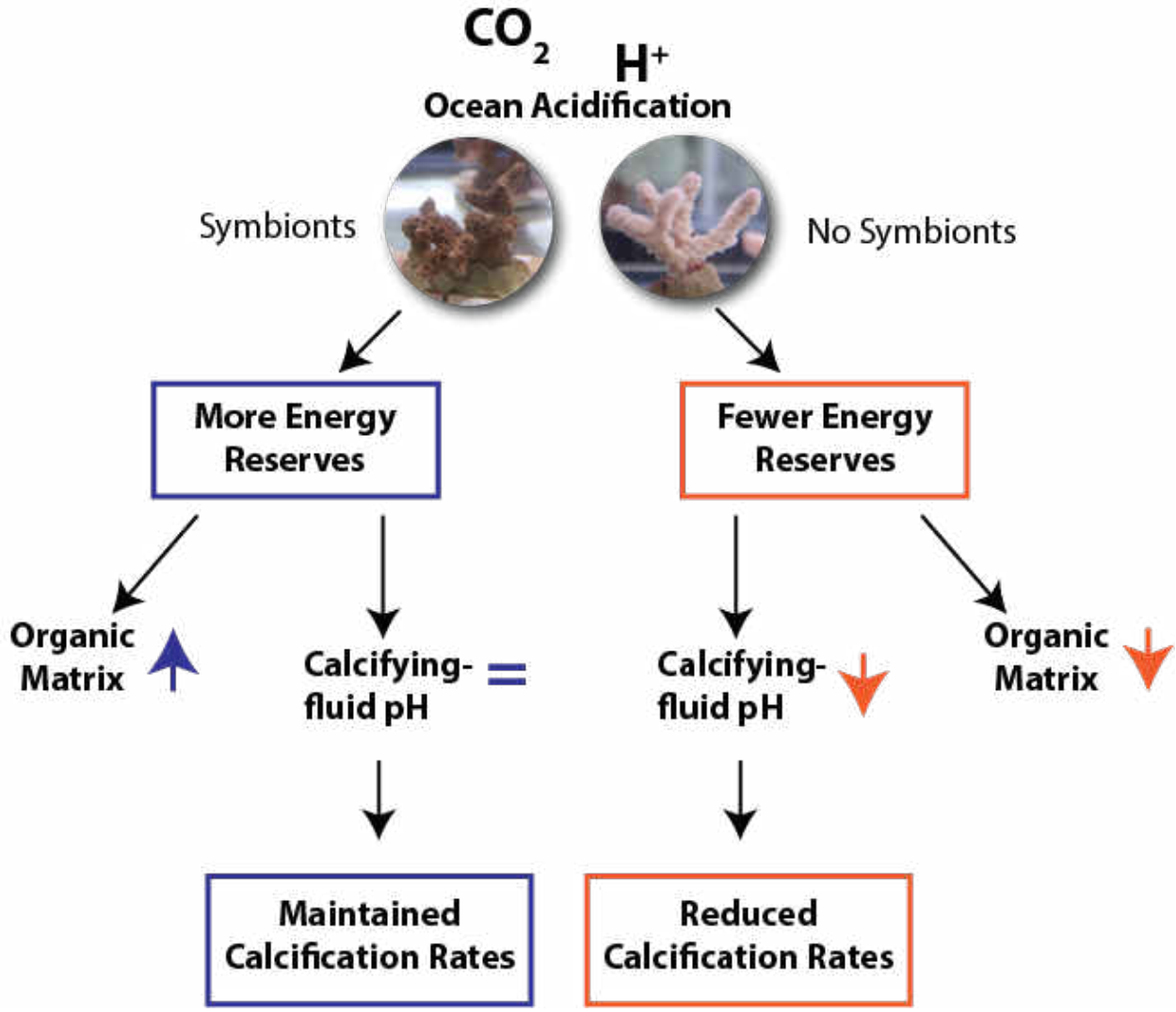

Figure 3. Flow chart following the predictions under the hypothesis that algal symbionts facilitate the acclimatization of *O. arbuscula* to OA. I predicted that more energy reserves continuously offered by symbiotic algae would allow the energy expenditure towards upregulation of calcifying fluid pH and organic matrix to maintain calcification rates when exposed to OA.

CHAPTER 2

METHODS

Coral Collection and Experimental Design

In May 2019, a total of 24 *O. arbuscula* colonies were collected from an artificial reef, the ship SS Addie Bagley Daniels (31° 36.207, -80° 47.750), 17.5 nautical miles off the coast of Georgia, U.S.A. To investigate the role of algal symbionts in coral resilience to OA, symbiotic and aposymbiotic colonies were collected for the experiment. Twelve dark brown colonies, indicative of the presence of algal symbionts (Figure 4a), were collected 16 m below sea level from the upper deck of the ship. Twelve aposymbiotic colonies, denoted in the field by their white coloration (Figure 4b), were collected at a depth of ~19 m, from the sides of the ship where they were shaded from sunlight by overhangs. Colonies were collected at least 1 m apart to increase the likelihood they were genetically distinct and were approximately 10-15 cm in diameter. The 24 colonies were transported to Georgia Southern University in separate seawater-filled plastic bags to keep genotypes separate and floated in a cooler containing seawater from the site of collection for temperature regulation. Water in the cooler was refreshed in between dives, prior to transport back to the dock, and again before driving from Savannah to Statesboro, Georgia. In the laboratory, corals were acclimated to room temperature (20°C) for 5 h and distributed among 4 aerated 38 L aquaria filled with artificial seawater (Instant Ocean). Symbiotic colonies were always kept separate from aposymbiotic colonies to prevent colonization of aposymbiotic coral tissue by algae. The initial densities of symbiotic algae in the symbiotic corals ranged from $2.09 \times 10^{5} \cdot cm^{-2}$ to $2.71 \times 10^{6} \cdot cm^{-2}$ and averaged $1.01 \times 10^{6} \cdot cm^{-2}$. For aposymbiotic corals the cell density ranged from $0 \cdot cm^{-2}$ to $1.20 \times 10^{4} \cdot cm^{-2}$, averaging $2.11 \times 10^{3} \cdot cm^{-2}$. Total chlorophyll concentrations of symbiotic corals ranged from 4.75 $\mu g \cdot cm^{-2}$ to 8.01 $\mu g \cdot cm^{-2}$ and averaged 2.96 $\mu g \cdot cm^{-2}$. For aposymbiotic corals chlorophyll ranged from 0 $\mu g \cdot cm^{-2}$ to 0.048 $\mu g \cdot cm^{-2}$ and averaged 0.002 $\mu g \cdot cm^{-2}$.

Two days after collection, each colony was divided into three fragments. One fragment was frozen (-80°C) to serve as the initial sample while the other two fragments were used for the pH exposure experiment. Coral fragments not frozen were epoxied to 4.7x4.7cm ceramic tiles using Z-Spar underwater

epoxy and allowed to recover for two days before being exposed to alizarin red sulfonic acid for 48 h to apply an initial skeletal mark (Lamberts 1973). Once stained with alizarin, twelve 38 L aquaria were assigned four corals each, where seawater was maintained at a salinity of 35 ppt, 26℃ and pH 8.0 or 7.6. The largest colonies were identified visually and distributed evenly among the aquaria to have similar biomass between aquaria. Colonies were otherwise assigned haphazardly, ensuring each genotype was represented in both a control and OA treatment. Corals were acclimated to a control temperature of 26℃ over 4 days. Before pH treatments began, initial skeletal weights were measured via buoyant weight. Fragments were hung by a 19 cm wire hook, fastened under an electronic balance (Sartorius R200D), into a seawater filled tank. Each coral was weighed 3 times to balance measurement variation due to water movement. Between each measurement the coral was removed from the hook and gently placed at the bottom of the tank, allowing the water to become still before zeroing the scale. The mean of these 3 weights was used for data analysis. Salinity (35ppt) and temperature (26℃) were kept constant throughout measurements to avoid alterations in seawater density. After obtaining colony weights, the pH was reduced from 8.0 to 7.6 in 6 aquaria at a rate of 0.1 pH units every 6 h. The control pH (8.0) signified the current ocean average and the acidification treatment of 7.6 was consistent with extreme projections for year 2100 (Noakes 2018; Pörtner et al. 2019).

Corals were fed twice a week with *Artemia sp.* nauplii within separate 5-liter containers floated in the seawater of each aquarium to keep aquarium water clean. Five mL of *Artemia* eggs were hatched in 1.4 L of seawater and a standard 0.1 L volume of this homogenized concoction was added to each feeding container. Corals remained within feeding bins until the water was visually clear of *Artemia,* usually within 2-4 h. Corals were then returned to their respective aquaria and water from the feeding bins discarded. Once each week the four corals within each aquarium were rotated one position clockwise to guard against placement effects. Aquaria were lightly scrubbed twice a week to prevent cyanobacterial or algal build-up and a 30% water change was completed once a week.

Artificial seawater (Instant Ocean) was made in a 189 L carboy using filtered, RO, and DI water. The alkalinity of the seawater was reduced to levels measured at GRNMS (2300μmol/Kg) by adding 10% HCl at least 24 h before the water was transferred to aquaria (Xue et al. 2016). The set-up of each aquarium consisted of an airstone, circulating pump (5 L/min), a power filter (physical and charcoal filters), and a 48 cm long LED light (11W; NICREW). Lights were mounted about 1 m above the surface of the water to prevent light induced bleaching and programed for a 10 h light:14 h dark cycle. Corals received an average of 4.86 ± 0.53 μmol photons m^{-2} s^{-1} quantified with a submersible Li-Cor quantum sensor (LI-192SA with LI-250A datalogger).

An Apex aquaria control system (Neptune, Inc.) was used to maintain experimental conditions (Table 1). Temperature and pH probes logged seawater conditions every 5 min. The system was programmed to control aquarium heaters to maintain a temperature of 26°C. In OA treatments, solenoid valves were opened when the pH rose above 7.6 allowing pure CO_2 to be bubbled into the seawater at one second intervals until the target pH was reached. pH probes were calibrated twice a week and water was collected after calibration to measure total pH spectrophotometrically using thymol blue (Zhang and Byrne 1996). Total pH was compared to pH probe readings at the time of water sample collection, and deviations from the total pH measurements were used to refine the pH control code, minimizing treatment deviation throughout the experiment (Table 1).

Aquaria salinities were recorded once per week using a refractometer and were maintained at 35ppt. Water samples were collected five times during the experiment from all 12 aquaria and total alkalinity analyzed with a Hanna instruments HI-901 automatic potentiometric titrator. Frequency of alkalinity measurements were constrained due to titrator failure during the beginning of the experiment. pCO_2 and aragonite saturation state were calculated using the CO2SYS (excel) program, with temperature, pressure, salinity, TA, and total pH measurements as inputs (Table 1; Dickson 2007).

Coral colony health was monitored each day, and any signs of bleaching recorded. Five days into the experiment, a solenoid valve malfunctioned and was found to be stuck open in one aquarium housing

symbiotic corals at pH 7.6. The pH quickly reached 7.1 but was returned to treatment range within 1.5 h. Afterwards significant bleaching started to occur. All four colonies in this aquarium were bleached by day 51 of the experiment and exhibited a negative percent change in buoyant weight. The four corals in this aquarium were omitted from further analysis.

The experiment was terminated after 51 days by removing the *O. arbuscula* fragments from the aquaria and measuring final buoyant weights as described above before placing them into a -80℃ freezer. Subsequent physiological and biochemical assays took place in the following order. One branch was removed from each coral for AFDW, lipid, and protein analysis. Another branch was removed to measure densities of symbiotic algae and chlorophyll concentrations. Tissue was removed from all remaining branches and linear extension measured before skeletal material was removed for either boron stable isotopes analysis or proteinaceous organic matrix. Due to the number of analyses completed and the small size of the *O. arbuscula* colonies, there was not enough skeleton remaining in all cases to carry out both organic matrix and boron analyses. Thus, a subset of individuals is represented for each of these assays.

Use of energy reserves in symbiotic and aposymbiotic colonies

After removing tissue by Waterpik for algal cell counts and chlorophyll measurements, the resulting slurry was centrifuged at 4500 rpm for 15 min to pelletize algal cells. A 10 µl subsample of supernatant was checked under a microscope (400x) for algal cells. The sample was centrifuged a second time if cells appeared in the supernatant. If the supernatant was clear of cells, it was decanted off. The algal pellet was then resuspended in 5 mL of DI water and vortexed until it appeared as a uniform color of brown throughout the liquid, with no visible clumps. A 1 mL aliquot of this sample was removed for symbiont cell counts and another 1.5 mL aliquot for determination of chlorophyll concentrations. Both of these samples were stored in a freezer at -20°C until ready to be analyzed. Densities of algal symbionts were quantified on a hemocytometer (Brightline) at 400x magnification. In order to reduce clumping of algal cells, thawed samples were vortexed for 10 seconds and then further mixed by pipetting the slurry up and down with a glass Pasteur pipette. A micropipette was used to load a 10µl subsample into the

hemocytometer counting chambers and 6 replicate slides were counted for each sample. The single largest outlier of these counts was discarded, and the mean cell density based on the other 5 counts was determined and normalized to surface area expressed as cells·cm^{-2}. All surface areas were quantified with the 3D Systems Capture^{TM} Mini 3D scanner using Geomagic Control X 64 software.

Chlorophyll was processed by first centrifuging tissue slurries at 14,000 rpm for 5 min to pellet the algae and then decanting the supernatant. Chlorophyll was extracted from the algal pellet over 24 h at 4°C with 1mL 100% HPLC grade acetone. On the second day samples were centrifuged at 14,000 rpm for 5 min and the supernatant was decanted into a clean tube and 0.5 ml acetone was added to the algal pellet to extract remaining chlorophyll. After 24 h, the sample was centrifuged at 14,000 rpm and the acetone supernatant was combined with the initial extraction to equal 1.5mL. The combined supernatant was centrifuged once more prior to measuring absorbance at 630 and 663 nm on a spectrophotometer (Shimadzu UV2600). Absorbance was used to calculate chlorophyll-a, chlorophyll-c and total chlorophyll normalized to surface area (μg·cm^{-2}) (Jeffrey and Humphrey 1975).

To assess the role of energy reserves in facilitating acclimatization of *O. arbuscula* to OA stress, one branch of approximately 3 cm length from each colony was freeze dried and pulverized in a SPEX ball mill. The resulting powder was subsampled for ash free dry weight (AFDW), lipids, and protein. Aliquots of the crushed skeleton of approximately 1 g were processed in duplicate for AFDW. AFDW samples were combusted at 500 °C for 12 h (ThermoScientific Thermolyne F56000), allowed to cool to room temperature in a glass desiccator and then weighed. AFDW was normalized to surface area (as determined with 3D Systems Capture^{TM}).

For each powdered coral fragment, triplicate aliquots of 0.15-0.30 g were measured for lipid extractions. Lipids were processed using a 20:1 solvent to sample ratio. The solvent consisted of 53.3% chloroform, 26.7% methanol, and 20% of 0.88% $NaCl_{(aq)}$. Initially, chloroform and methanol were added to samples that were then placed on an orbital sample agitator. After extracting for 2 h skeletal matter was removed by passing the sample through filter paper with a pore size of 11 μm. $NaCl_{(aq)}$ was then added to

wash any impurities out of the sample. After centrifuging at 1500 rpm for 5 min to speed up the separation of density layers, methanol and $NaCl_{(aq)}$ at the top were removed using a glass Pasteur pipette, and the remaining chloroform solution was dried with a steady stream of N_2 in a heat block at 30°C. Total lipids were determined by weight and normalized to AFDW (Grottoli-Everett and Kuffner 1995). Normalizing lipid and protein storage to tissue biomass is more robust because the penetration of tissue into the skeleton of each coral species can be different (Edmunds and Gates 2002; Grottoli et al. 2004). This allows for better comparison across studies.

The crushed coral sample that was used for AFDW and lipids was also subsampled for total protein analysis in aliquots of 0.05g. Skeletal powder was sonicated in 1.5ml Milli-Q water for 2 min to detach coral tissue from the skeletal particulate. After sonication, samples were centrifuged for 10 min at 5000 rpm at 4°C to separate the skeletal material from the protein. Following centrifugation, the supernatant was decanted and the sample was lyophilized for 12 h. Protein was solubilized with 0.5 ml of 0.1 N NaOH at 30 °C for 1 h with the samples shaken briefly every 15 min. Total protein was determined with the bicinchoninic acid assay method with standard curves made from bovine serum albumin (Pierce BCA Protein Assay Kit; (Smith et al. 1985)). All samples and standards were run in triplicate, with a 96-well microplate spectrophotometric plate reader (Molecular Devices© SpectraMax M3). Total protein was determined as the mean of the three measures and normalized to AFDW.

Modulation of calcifying fluid pH and organic matrix production

To investigate mechanisms employed by *O. arbuscula* to control calcification, I first assessed variability in calcifying fluid pH between treatments using boron isotopes. The amount of borate ($B(OH)_4^-$) incorporated into the skeleton is directly related to the pH of the calcifying fluid (equation 4; Dickson 1990; Egleston et al. 2010). As described previously, borate can be quantified by measuring the stable isotope ratios of boron 11 to boron 10, which changes due to fractionation (page 11). As the pH of calcifying fluid decreases there will be a corresponding decrease in relative abundance of boron 11 ($\delta^{11}B$).

For stable isotope preparation, ~8 mg of apical skeletal growth during the experiment, as denoted by the presence of skeleton above the alizarin red stain line, was removed using a hand file. Tissue was

removed from the skeleton by incubating the sample in 6% sodium hypochlorite for 12 h at 4°C. Samples were centrifuged and supernatant discarded. The clean skeletal powder was rinsed three times with DI water, with the sample centrifuged each time and the supernatant pipetted off after each rinse. Once in the boron free lab space at the University of South Carolina Center for Elemental Mass Spectrometry, skeletal samples were sonicated three times in boron free water. Skeletal powder (8 mg, ~400 ng B) was dissolved in 75µl of 3M HNO_3 in a laminar flow lab bench with a B-free HEPA filter. Boron purification followed the micro-sublimation method of Wang et al. (2010). The dissolved sample was transferred onto the inner surface of Teflon vial caps, hand tightened and placed into metal wells on the top of a hotplate. These vials were incubated for 24 h at 100°C to sublimate the sample droplet to the top of the conical vial (Gaillardet et al. 2000). Vials were weighed before and after sublimation, monitoring mass loss in order to screen isotope outputs for outliers. Due to Rayleigh distillation, if mass loss is too high, the sample will be enriched in boron 11 because the lighter isotope 10 will preferentially evaporate. Mass loss during micro-sublimation was typically ~5%, a level of which was confirmed to produced negligible fractionation

In preparation for analysis the distillate was transferred to clean autosampler vials and diluted to a volume of 575 µl using 0.3M hydrofluoric acid (HF). The boron concentrations were determined semi-quantitatively by dip sampling the diluted samples and monitoring the voltage of boron 11 on the Neptune MC-ICP-MS. All standards could then be diluted to match the sample concentration. A non-experimental branch of *O. arbuscula* was pulverized for a consistency standard that was run along each set of samples to assess day to day machine drift. Dilutions of the boron isotopic standards, National Bureau of Standards 951 (NBS 951), JAB-B and SRM 8301 (Stewart et al. 2021) were made in a mixture of 0.26M HNO_3 + 0.29M HF and were matched to average sample concentrations. Blank solutions were made up of 0.26M HNO_3 + 0.29M HF. All standards and samples were diluted in the same concentrations and proportions of acids.

Boron ratios ($^{11}B/^{10}B$) were determined according to the methods outlined in Foster (2008) using a multiple collector inductively coupled plasma mass spectrometer (Thermo Neptune MC-ICP-MS;

CEMS Columbia, SC). The inlet system was comprised of a 100µl/min µflow PFA nebulizer, a cyclonic spray chamber, a platinum JET cone, and a nickel X-skimmer cone (Table 2). Sample gas, torch position, and lenses were tuned for maximum sensitivity. A routine was then performed to determine the relationship between sample gas rate and $^{11}B/^{10}B$ ratios, and the sample gas rate was set to where the slope was lowest, generally 90% of maximum sensitivity. On-peak baselines were measured on the blank solution of HF and HNO_3 prior to each analytical session. Isotope ratios were measured for 30 cycles at four seconds per cycle. Mass bias was externally corrected for using a standard sample bracket (SSB) approach, by running NBS 951 before and after each sample, and calculating the square root of the sum of squares of each error (Foster 2008; Wang et al. 2010). Accuracy and precision were monitored by SSB runs of NBS 951 and JAB-B every 8 samples and at the start and end of each session. The blank solution was run before and after a set of 4 SSB runs, and $^{11}B/^{10}B$ ratios were calculated after subtracting the average of the blanks. Blanks were approximately 0mV at the start of each session and increased to about 7mV for boron 11, which was roughly 0.1% of signals measured during SSB runs.

Several replicates of an in-house boric acid standard (Alfa Aesar B elemental standard) were run at the beginning and end of each analytical session to monitor instrumental uncertainty. Over the 5-month period when these samples were analyzed, replicate analyses of the in-house standard yielded +0.29 ± 0.15‰ (2σ, n=62). Several replicates of the NIST SRM 8301 (coral) standard yielded +24.00 ± 0.15‰ (2σ, n=6), which is within analytical error of the certified value of 24.17 ± 0.18‰ (2σ; Stewart et al., 2021). A total procedural blank was run during each analytical session, which averaged 60 pg B (less than 0.02% of the average micro-sublimated sample size).

In addition to assessing relative calcifying fluid pH via boron stable isotopes, I quantified proteinaceous organic matrix in *O. arbuscula* skeletons as a second biological mechanism potentially facilitating the calcification process under OA stress. Unfortunately, due to unforeseen circumstances (i.e., building infrastructure failure) that caused early termination of the laboratory experiment, there were a limited number of replicates available for this analysis. Therefore, *O. arbuscula* skeletons used for assessing the impact of pH on organic matrix production came from two sources. Specifically,

aposymbiotic colonies used for this assessment were from the present experiment, whereas symbiotic colonies were from a previous experiment reported in Wang et al. (2020). Symbiotic *O. arbuscula* colonies from Wang et al. (2020) were collected from J-Y reef (31° 36.056, 80° 47.431), a hard bottom site adjacent to the ship SS Addie Bagley Daniels where corals in the current study originated. Coral colonies in the Wang et al. (2020) study were exposed to ambient (8.0) and low (7.8) pH by maintaining pCO_2 conditions of 420 and 1000 ppm, respectively, with a mass flow (Aalborg) controller and infrared gas analyzer (LiCor LI-840A). Seawater variables such as water temperature (26℃), alkalinity (2.3 mM), and salinity (35 ppt) were similar to those maintained in the present experiment (Table 1).

For both symbiotic and aposymbiotic colonies approximately 100 mg of apical skeletal growth were removed using a hand file. Powdered samples were allowed to incubate in 6% sodium hypochlorite for 12 h at 4℃ to remove organic material associated with the coral tissue or any other external sources. Samples were centrifuged for 2 min at 8000 rpm and the supernatant discarded. To ensure complete removal of the coral tissue, 1M NaOH was added to the pellet and observed for reactivity indicated by bubbles. If bubbles were not present, samples were again centrifuged, and the supernatant pipetted off. If the NaOH solution appeared to be reacting with remnant tissue in the sample, NaOH was again added and the process repeated until the solution appeared clear and free of bubbles. The clean skeletal powder was rinsed 3 times with DI water, with the sample centrifuged and the supernatant pipetted off after each rinse.

The washed skeletal powder was freeze dried and the final mass of each sample recorded before decalcifying in 1N HCl at room temperature with constant stirring. HCl was added in volumes of 1 mL at 10 min intervals until the powder was fully dissolved and production of bubbles ceased. This solution was then brought to a neutral pH by adding 0.5 M NaOH in 50 µl increments until a pH of 7.0 was reached (Drake et al. 2013)).

Following the procedure detailed in Rahman et al. (2011), organic matrix was isolated from the skeletal solution by first pre-filtering through a 0.2 µm polyethersulfone syringe filter and then passing the filtrate through two, methanol primed and rinsed Waters C-18 Sep-Paks connected in series. The Sep-

Paks were rinsed with 30 mL DI water, followed by 6 mL 10% acetonitrile. Finally, macromolecules were eluted and collected in a clean vial with 6 mL of 50% acetonitrile. Eluted macromolecules were frozen at -80°C and lyophilized before continuing with the Bradford micro assay (Pierce™ Coomassie (Bradford) Assay Kit; Smith et al. 1985; Tambutté et al. 2015). Protein was incubated in 0.5 mL of 0.1M NaOH for 1 h at 30°C, shaking every 15 min. All samples and bovine serum albumin standards were run in triplicate, with a 96-well microplate spectrophotometric plate reader (Molecular Devices© SpectraMax M3). Total proteinaceous organic matrix was normalized to skeletal mass ($ug \cdot g^{-1}$).

Calcification rate response

Calcification rates were determined via buoyant weight and linear extension. Buoyant weight was calculated as percent change during the 51-day experiment. Buoyant weight was measured on day 0 and day 51 to the nearest 0.1 mg and calculated as percent change during the 51-day experiment as described above (page 18; Davies 1989). Linear extension was measured above the initial alizarin skeletal stain after coral tissue was removed. Corals were placed under a stereomicroscope fitted with a camera and length was measured on the computer-projected image (Axiocam ERc 5s; Zen Blue v2.5). Measurements were corrected for magnification and the mean linear extension per day from all branches on each coral fragment was used in statistical analyses of growth. Finally, skeletal densities were calculated using the increase in buoyant weight during the 51 day experiment divided by the average total linear extension.

In situ site experiment

The *in situ* experiment investigating calcification rates and regulation of calcifying fluid pH in *O. arbuscula* was conducted within the boundaries of Gray's Reef National Marine Sanctuary (GRNMS). This sanctuary occurs ~20 nm off the coast of Georgia, U.S. and possesses a CO_2 monitoring system that has been in place for over a decade logging data from both the seawater surface and seafloor. This monitoring demonstrates that pCO_2 and pH fluctuate naturally on a seasonal basis. pCO_2 is elevated during the summer through autumn months, corresponding to rising temperatures, storms, and freshwater

intrusion from numerous estuarine rivers (Wanninkhof et al. 2015). During the winter, carbon remains stored in the seawater's carbonate chemistry, mostly bicarbonate and carbonate. Warmer temperatures reverse this process resulting in more CO_2 in the seawater, so much so that seawater will often vent excess CO_2 into the atmosphere during summer months (Noakes 2018). Currently pCO_2 reaches upwards of 1000 µatm and pH levels as low as 7.8 during these warm months. Additionally, benthic organisms sometimes experience more intense spikes in pCO_2 than measured at the sea surface. During low pressure systems of coastal storms, CO_2 is released from sediment pores increasing pCO_2 and decreasing pH on the seafloor that is not detected by the monitoring buoy at surface waters (Noakes 2018).

To test the response of *O. arbuscula* to natural fluctuations in pCO_2 and corresponding pH, in August 2018, 26 coral fragments approximately 6 cm in length were collected from separate colonies via SCUBA outside of the research area within GRNMS. Aboard the R/V Nancy Foster, coral fragments were stained with Alizarin Red for 48 h within a 38 L aerated aquarium fitted with an 11W LED light above the water. On the third day after collection, 20 of the stained corals were secured to a PVC plate fastened between the CO_2 and water quality sensors at 18 m depth in the north end of GRNMS (31˚ 24.159N, 80˚ 52.210W; Figure 5). The remaining six fragments were kept as initial samples. Six of the 20 corals were collected in each of the following months: December 2018, May 2019, and November 2019. The pCO_2 ranged from 455 to 1052 µmol · mol^{-1} in the spring and summer months. In the autumn and winter pCO_2 ranged from 392 to 1166 µmol · mol^{-1} (Figure 6; Table 3). Temperatures ranged from a maximum of 31.4℃ during the summer to a minimum of 12.9℃ during the winter. From August to December 2018, and May to October 2019 raw pH data was available from the sensors on the GRNMS seafloor. pH sensor data was not available for March-May 2019, and October-November 2019. pH values from those intervals were instead calculated with CO2SYS using pCO_2, temp, salinity, alkalinity, and pressure recorded on the seafloor. Pre-august 2018, the seafloor sensors were not yet deployed for the year, so values were collected from the seawater-surface buoy data and pH was calculated using CO2SYS.

Boron isotopes were analyzed using the protocol outlined previously and isotopic measurements were used to calculate the calcifying fluid pH (pH_{boil}) using the boron pH proxy (equation 5), where pK_B is the well-defined dissociation constant of 8.597 at 25 °C and 35 psu (Dickson 1990), $\delta^{11}B_{sw}$ represents the amount of ^{11}B in seawater which is a value of 39.5 (Foster 2008), $\delta^{11}B_{carb}$ is the amount of ^{11}B measured in the carbonate, and α is the fractionation factor for boron of 1.0272, most commonly used in boron proxy literature (Klochko et al. 2006) (Krief et al. 2010; Trotter et al. 2011; Anagnostou et al. 2012; McCulloch et al. 2012).

$$pH_{biol} = pK_B - log\left\{\frac{\delta^{11}B_{sw} - \delta^{11}B_{carb}}{\alpha \times \delta^{11}carb - \delta^{11}Bsw + 1000(\alpha - 1)}\right\} \quad (5)$$

Statistical Analyses

All variables were tested for normality using the Shapiro-Wilk W test and equal variance with Levene's test (JMP). Data that did not meet assumptions were log or square root transformed. Initial samples were used to measure differences in energy reserves between symbiotic and aposymbiotic colonies. A paired t-test was used to assess differences in densities of algal symbionts and chlorophyll concentrations between genotypes under each pH condition. A repeated measures ANOVA was used to assess variation in temperature, pH, TA, and pCO_2 within each treatment over time. Two-way ANOVAs, using the expected means square model with aquarium number as random effect, incorporated symbiont status and pH treatments as factors to test for significant differences in % calcification, AFDW, protein, total lipids, and $\delta^{11}B$. In order to complete the two-way ANOVA, the mean for the four corals from each aquarium was used for analysis resulting in n=3 for each treatment except for the symbiotic coral at low pH treatment where n=2. Proteinaceous organic matrix of symbiotic and aposymbiotic corals were assessed separately since the samples came from different experiments. The samples from low pH treatments were compared to their respective control samples using a nested-ANOVA, where individual samples were nested within replicate aquaria. For the *in situ* site experiment, a linear regression was performed to test the relationship between seawater pH and upregulation of calcifying fluid pH (ΔpH) by *O. arbuscula* at GRNMS.

Table 1. Experimental conditions in aquaria, including temperature and carbonate chemistry parameters, averaged over the course of the laboratory experiment with *O. arbuscula* (±s.d). n=3 for all treatments except symbiotic corals at 7.6 pH where n=2. Sym = symbiotic corals, Apo = Aposymbiotic corals

Treatment	pH_T	T.A. (µmol/KG)	pCO_2 (ppm)	Ω_{arag}	Temp. (°C)
8.0 - Sym	7.94 ± 0.09	2155 ± 120	475.3 ± 50.04	2.8 ± 0.29	26.0 ± 0.01
8.0 - Apo	7.96 ± 0.07	2290 ± 126	470.1 ± 78.45	3.1 ± 0.43	25.9 ± 0.17
7.6 - Sym	7.64 ± 0.11	2221 ± 88	1125.7 ± 243.75	1.6 ± 0.38	26.03 ± 0.05
7.6 - Apo	7.62 ± 0.15	2301 ± 146	1229.3 ± 307.42	1.6 ± 0.38	26.04 ± 0.15

Table 2. Neptune MC-ICPMS operating conditions

Parameter	Variable	Setting
MC-ICPMS		
	Instrument	Neptune with Plus upgrade
Interface		
	Nebulizer	PFA, 100 µl/min
	Spray chamber	Cyclonic
	Sample cone	Pt, Jet configuration
	Skimmer cone	Pt, X configuration
ICP ion source		
	Power	1200 W
	Cooling gas flow rate	16 L/min
	Auxillary gas flow rate	0.8 L/min
	Sample gas flow rate	1.00-1.05 L/min
	Additional gas flow rate	0.02-0.05 L/min
Mass spectrometer		
	Ion energy	10,000 V
	Extraction energy	2,000 V
	Analysis mode	Static
	Ion detection	Analogue by Faraday
	Typical sensitivity	15 V/ppm B
	Integration time	4 s
	Settling time	3 s
	Cycles per run	30

Table 3. Average sea water conditions at the Gray's Reef National Marine Sanctuary site where *O. arbuscula* were secured to the water quality monitoring instrument platform and allowed to remain for either 4, 9, or 15 months prior to collection for skeletal boron isotope analysis. *Denotes that pH was calculated using CO2sys with other recorded water quality parameters rather than directly measured by the *in situ* pH probe.

Season	Months	Median pCO_2 (µatm)	Average pH	Average Temperature (°C)
*Summer	Jun-Aug	553.23	7.92	28.63
Winter	Oct-Dec	571.87	7.98	21.28
*Spring	March-May	700.56	7.83	17.81
Autumn	Sept-Nov	663.91	8.0	27.69

a)  b) 

Figure 4. *Oculina arbuscula* colonies a) symbiotic with indicative dark brown coloration and b) aposymbiotic with transparent tissue reflecting lack of algal symbionts.

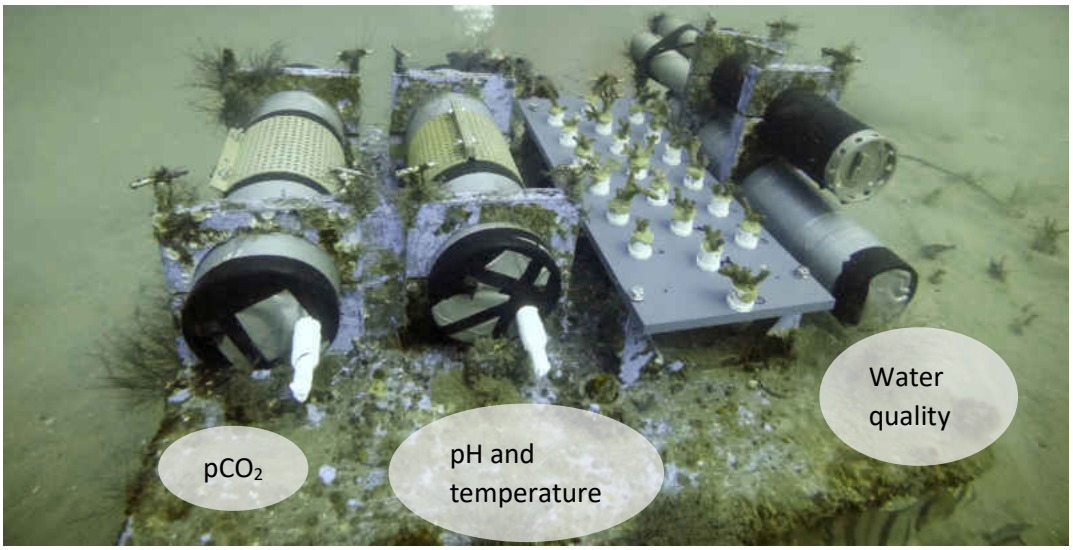

Figure 5. Seafloor water chemistry monitoring system at GRNMS with a PVC plate holding *O. arbuscula* fragments to the right of the pCO_2 and pH sensors. To the right of the coral fragments is the water quality system measuring salinity and dissolved oxygen.

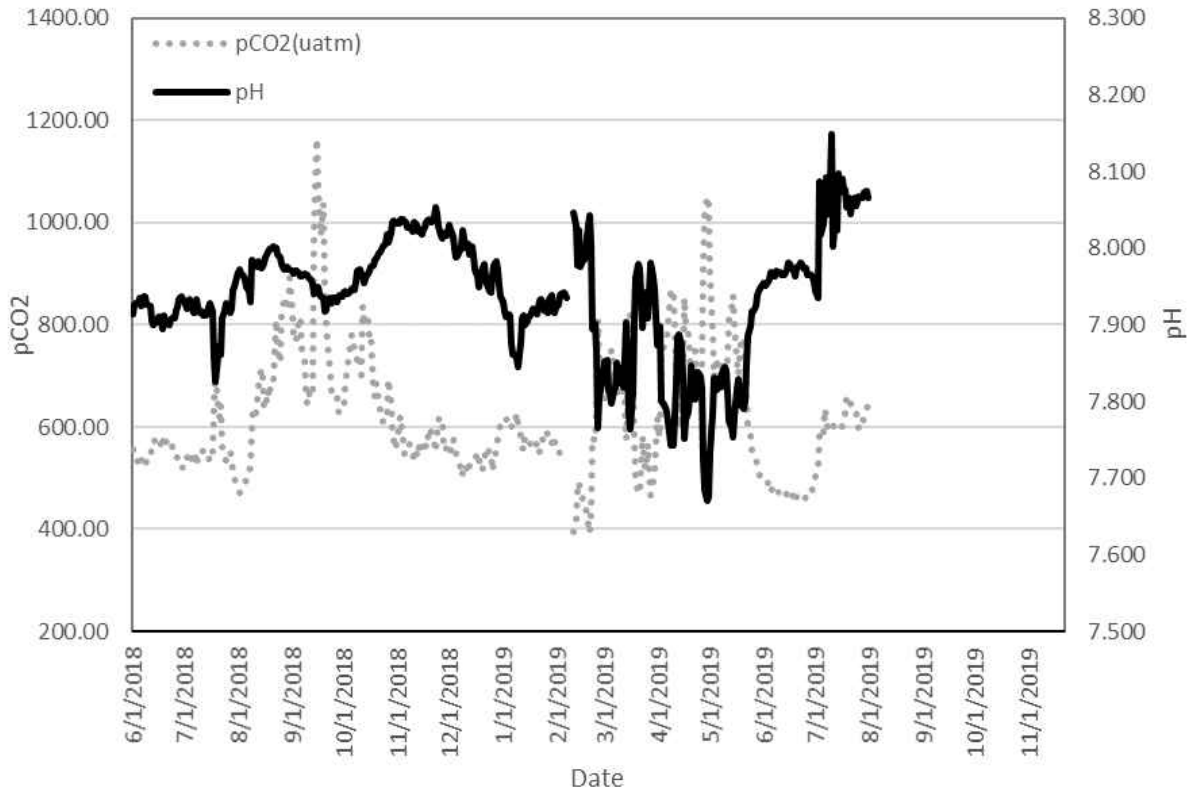

Figure 6. Partial pressure of CO_2 and pH recorded at the GRNMS monitoring station for the time period that skeletal growth measurements were taken for *O. arbuscula* in the *in-situ* field trial, June 2018 – November 2019.

CHAPTER 3

RESULTS

Coral colonies maintained good health throughout the 51-day experiment based on daily observations of tentacle and polyp extension along with active feeding. All symbiotic corals maintained a deep-brown color suggesting high symbiotic algal densities, with the exception of the colonies in one low pH treatment aquarium where a solenoid valve malfunctioned and decreased the pH to 7.1 for 1.5 h. Corals in this aquarium were likely also impacted by a water leak from the aquarium room ceiling that damaged the pCO_2 control system, causing early termination of the experiment. Whereas *O. arbuscula* colonies in all other aquaria appeared to be healthy, coral fragments in the one low pH tank bleached and exhibited tissue loss. As a result, data from the four colonies in the aquarium impacted by the water leak were subsequently removed from final data analysis.

Seawater Chemistry

Throughout the 51 day experiment pH was significantly lower and pCO_2 significantly higher in OA versus control aquaria (Figure 7a&b; Table 4). Total alkalinity (TA) was not significantly different within or among treatments (Table 4) but did decrease during the experiment until day 34. During the latter portion of the experiment, I adjusted the alkalinity of the artificial seawater carboy to counteract alkalinity draw down which then resulted in increases in total alkalinity from day 34 to 51 (Figure 7; $p=0.0026$). While not significant, total alkalinity tended to be lower in the aquaria holding symbiotic corals, possibly caused by photosynthesis of the symbiotic algae drawing down bicarbonate at a faster rate (Figure 7c).

Use of energy reserves in symbiotic and aposymbiotic colonies

The densities of algal cells and corresponding chlorophyll concentrations in aposymbiotic *O. arbuscula* remained low and markedly different from symbiotic colonies during the laboratory experiment (Figure 8). Further, paired t-tests comparing genotypes in their respective low pH and control tanks

indicated that neither symbiotic algal densities nor chlorophyll concentrations were impacted by seawater pH (Table 5).

AFDWs were similar across all pH and symbiont combinations (Figure 9a; Table 6) whereas protein concentrations scaled by AFDW were impacted by the presence of symbionts, independent of pH. Specifically, protein reserves were significantly higher in aposymbiotic than symbiotic corals (Figure 9b; Table 6). While lipid concentrations were not significantly different between pH or symbiont treatments, there was a trend for greater lipid concentrations in symbiotic versus aposymbiotic corals (Figure 9c; Table 6). These differences detected in protein and lipid concentrations were not a carry-over from differences that were present initially as evidenced by the fact that energy reserve concentrations from initial samples did not differ significantly between symbiotic and aposymbiotic colonies (Table 7).

Modulation of calcifying fluid pH and production of organic matrix

$\delta^{11}B$ was used as a relative measure of the upregulation of calcifying fluid pH. Coral colonies maintained in a seawater pH of 7.6 had significantly higher $\delta^{11}B$ than in corals growing in a seawater pH of 8.0 (Figure 10; Table 8). Skeletal $\delta^{11}B$ in fragments of paired genotypes at pH 7.6 were on average 1.7‰ higher than the same genotype grown at pH 8.0, indicating a higher absolute calcifying fluid pH. In contrast, the presence or absence of algal symbionts had no significant impact on $\delta^{11}B$ and there was no evidence of an interaction between pH and symbiont status (Table 8). Uncertainty produced during mass spectrometry analysis of boron was ~0.15 ‰, an acceptable range for boron to indicate pH change.

As detailed in the methods, proteinaceous organic matrix was quantified from aposymbiotic *O. arbuscula* colonies in the present study and from symbiotic colonies investigated in a previous OA study (Wang et al. 2020). Reductions in pH had no effect on the concentrations of organic matrix in the skeletons of either aposymbiotic colonies or symbiotic coral colonies (Figure 11a & b; Table 9).

Calcification rate response

All corals included in the data analysis exhibited positive growth rates over the 51 day experiment (Figure 12). Corals held at a pH of 7.6 calcified 24% slower as measured by buoyant weight

than control colonies at a pH of 8.0 (Figure *12*). While statistical analysis indicated these differences were not significant, a trend was revealed. Percent changes in buoyant weight were similar between symbiotic and aposymbiotic corals. In contrast, linear extension rates were 1.4 times faster in aposymbiotic corals and symbiotic corals had 1.5 times denser skeletons than aposymbiotic corals (Figure 12). There were no interacting effects of pH and presence of symbiotic algae in any of the skeletal growth measurements (Table 6).

In situ measurements of boron 11 and calcifying fluid pH upregulation

Mortality occurred in only two of the 20 *O. arbuscula* colonies growing at the pCO_2 monitoring system between June and November 2019. By inputting skeletal $\delta^{11}B$ results into the boron pH proxy (equation 5), I found that the upregulation of calcifying fluid pH (ΔpH) in *O. arbuscula* throughout the year was dependent on the ambient seawater pH (Figure 13). This relationship was an inverse function where each unit decrease in ambient seawater pH was countered by an approximate one unit upregulation in calcifying fluid pH by *O. arbuscula* (slope= -0.982). Thus, the greatest differences between seawater and calcifying fluid pH were detected during the summer and spring months when seawater pH was lower. In the winter when seawater pH was "normal" the average upregulation was only about 0.59. However, when the average seawater pH dropped into the range of 7.9-7.8, upregulation resulted in a calcifying fluid pH that was 0.70 greater than the surrounding water.

Table 4. Repeated measures ANOVA for 4 water quality variables over time (n = 3 for all treatments except symbiotic corals at pH 7.6 where n=2). * denotes significant p-values, α=0.05.

Variable	F	NumDF	DenDF	p-value
Temperature				
Among treatments	1.2216	3	7	0.3707
Within treatments	0.5805	6.1913	14.446	0.454
Day	0.8427	2.0638	14.446	0.454
Among x day	0.5805	6.1913	14.446	0.7447
pH				
Among treatments	344.914	3	7	<0.0001*
Within treatments	2.3502	6.838	15.955	0.0755
Day	0.9384	2.2793	15.955	0.4229
Among x day	2.3502	6.838	15.955	0.0755
Total Alkalinity				
Among treatments	2.3717	3	7	0.1564
Within treatments	0.8393	4.3318	10.107	0.5379
Day	13.1328	1.4439	10.107	0.0026*
Among x day	0.8393	4.3318	10.107	0.5379
CO_2				
Among treatments	235.9501	3	7	<0.0001*
Within treatments	6.2614	8.1229	18.953	0.0005*
Day	10.235	2.7076	18.953	0.0004*
Among x day	6.2614	8.1229	18.953	0.0005*

Table 5. Results of paired t-test grouped by coral genotypes comparing densities of symbiotic algae and chlorophyll concentrations between control and low pH treatments in *O. arbuscula* after 51 days. The symbiont density data (cells cm^{-2}) did not meet normality assumptions and were transformed by log(x+1). Chlorophyll concentrations for the aposymbiotic corals were square root transformed to meet normality assumptions.

Variable	DF	t-ratio	p-value
Symbiotic			
Algal densities (cells cm^{-2})	7	1.133142	0.2945
Chlorophyll concentrations (µg cm^{-2})	7	0.812275	0.4434
Aposymbiotic			
Algal densities (cells cm^{-2})	11	1.61804	0.2699
Chlorophyll concentrations (µg cm^{-2})	11	1.725651	0.1124

Table 6. Two-way ANOVAs for *O. arbuscula* energy reserves (ash free dry weight (AFDW), total lipids, and total protein) and growth (buoyant weight, linear extension, and skeletal density) in response to control (8.0) versus low (7.6) pH over 51 days (n = 12 for all treatments except symbiotic corals at low pH where n=9). AFDW and lipids did not meet normality assumptions so were log transformed prior to analysis. *, $p < 0.05$

Variable	Numerator mean square	Numerator Degrees of Freedom	Denominator Degrees of Freedom	F-Ratio	p-value
AFDW					
pH	0.00576	1	7.094	0.0697	0.7994
Symbionts	0.01786	1	7.094	0.2161	0.6562
pH*Symbionts	0.00033	1	7.094	0.0040	0.9516
Protein					
pH	585.558	1	7.133	0.732	0.4200
Symbionts	5611.91	1	7.133	7.0368	0.0329*
pH*Symbionts	237.41	1	7.133	0.2977	0.6023
Lipid					
pH	0.6461	1	6.931	0.7274	0.4220
Symbionts	3.7706	1	6.931	4.2449	0.0784
pH*Symbionts	0.0024	1	6.931	0.0003	0.9874
Buoyant Weight					
pH	2.4413	1	7	4.9239	0.062
Symbionts	4.0603	1	7	2.9606	0.129
pH*Symbionts	0.03452	1	7	0.0419	0.8437
Linear Extension					
pH	140.671	1	7	3.4201	0.1069
Symbionts	487.685	1	7	11.8572	0.0108*
pH*Symbionts	30.9945	1	7	0.7536	0.4141
Skeletal Density					
pH	1.53×10^{-8}	1	7	0.1958	0.6714
Symbionts	7.83×10^{-7}	1	7	10.0188	0.0158*
pH*Symbionts	1.54×10^{-8}	1	7	0.1970	0.6706

Table 7. Results of t-tests comparing energy reserves in symbiotic and aposymbiotic *O. arbuscula* colonies prior to initiation of pH experiments. Data were generated by removing a branch from each colony prior to initiation of experimental conditions.

Initial Samples	DF	t-Ratio	p-value
AFDW	22	-0.37761	0.7093
Lipid	20	-0.61838	0.5433
Protein	22	0.03206	0.9747

Table 8. Two-way ANOVA results for the relative abundances of $\delta^{11}B$ in symbiotic and aposymbiotic *O. arbuscula* skeletons after exposure to ambient (8.0) and low (7.6) pH seawater for 51 days. *p<0.05.

Variable	DF	F-Ratio	p-value
δ11B			
pH	1	21.7916	0.0013*
Symbionts	1	1.2320	0.2973
pH*Symbionts	1	2.8839	0.1255

Table 9. Nested ANOVAs (α=0.05) comparing proteinaceous organic matrix in symbiotic *O. arbuscula* colonies exposed to pH of 8.0 and 7.8, and aposymbiotic colonies exposed to pH of 8.0 and 7.6.

Experiment	DFDen	F-ratio	p-value
Present Study			
Aposymbiotc Organic Matrix	1	0.0769	0.7953
Wang et al. 2020			
Symbiotic Organic Matrix	1	1.0870	0.3639

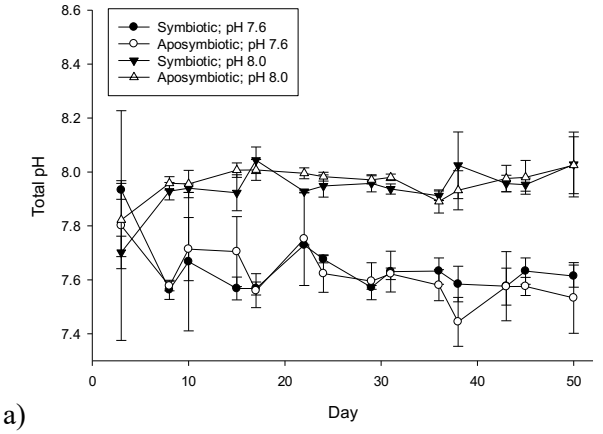

a)

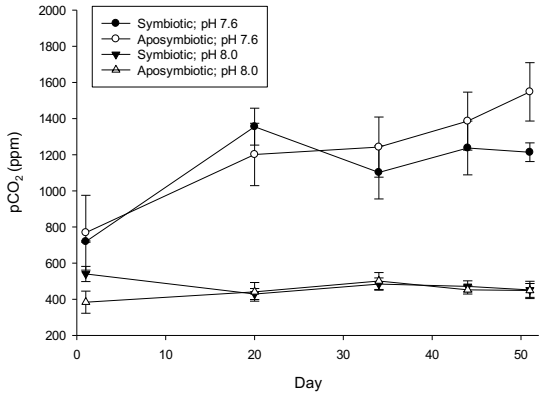

b)

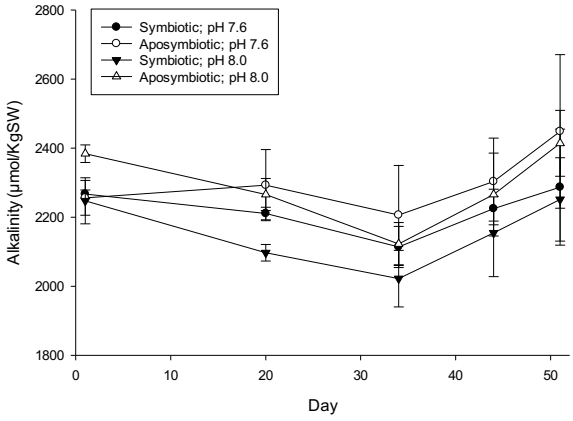

c)

Figure 7. Mean (±s.d.) of a) total pH, b) CO_2 concentrations, and c) Total Alkalinity (TA) of ambient (8.0) and low pH (7.6) treatments over the 51 day experimental period (n=3 for all treatments except symbiotic corals at low pH where n=2). CO_2 concentrations were calculated in CO2SYS MS Excel Program (by Pierrot, DE, Lewis, E, Wallace, DWR; https://cdiac.ess-dive.lbl.gov/ftp/co2sys/CO2SYS_calc_XLS_v2.1/) for the days TA was measured.

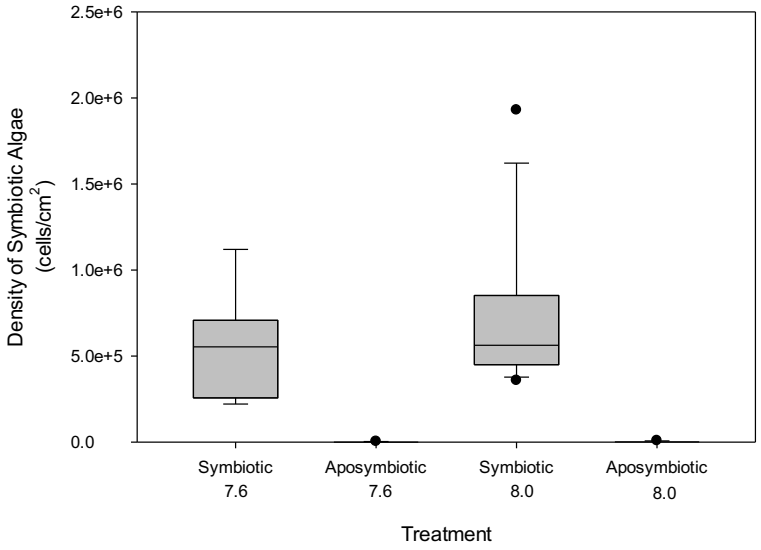

a)

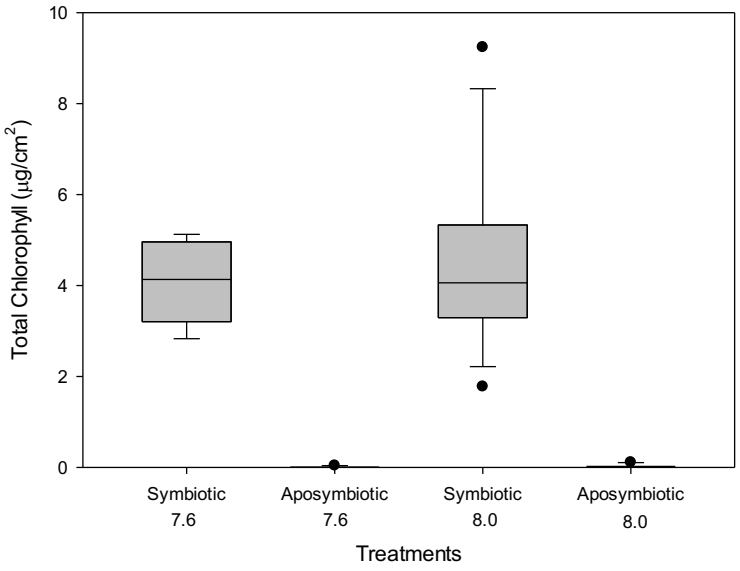

b)

Figure 8. Densities of symbiotic algae and chlorophyll concentrations of symbiotic and aposymbiotic *O. arbuscula* colonies in control pH (8.0) and low pH (7.6) for 51 days. The lower and upper bounds of the boxes indicate the 25th and 75th percentiles, and the extent of the whiskers indicates the 10th and 90th percentiles (n = 12 for all aposymbiotic corals and symbiotic corals at pH 8.0, n=9 for symbiotic corals at pH 7.6).

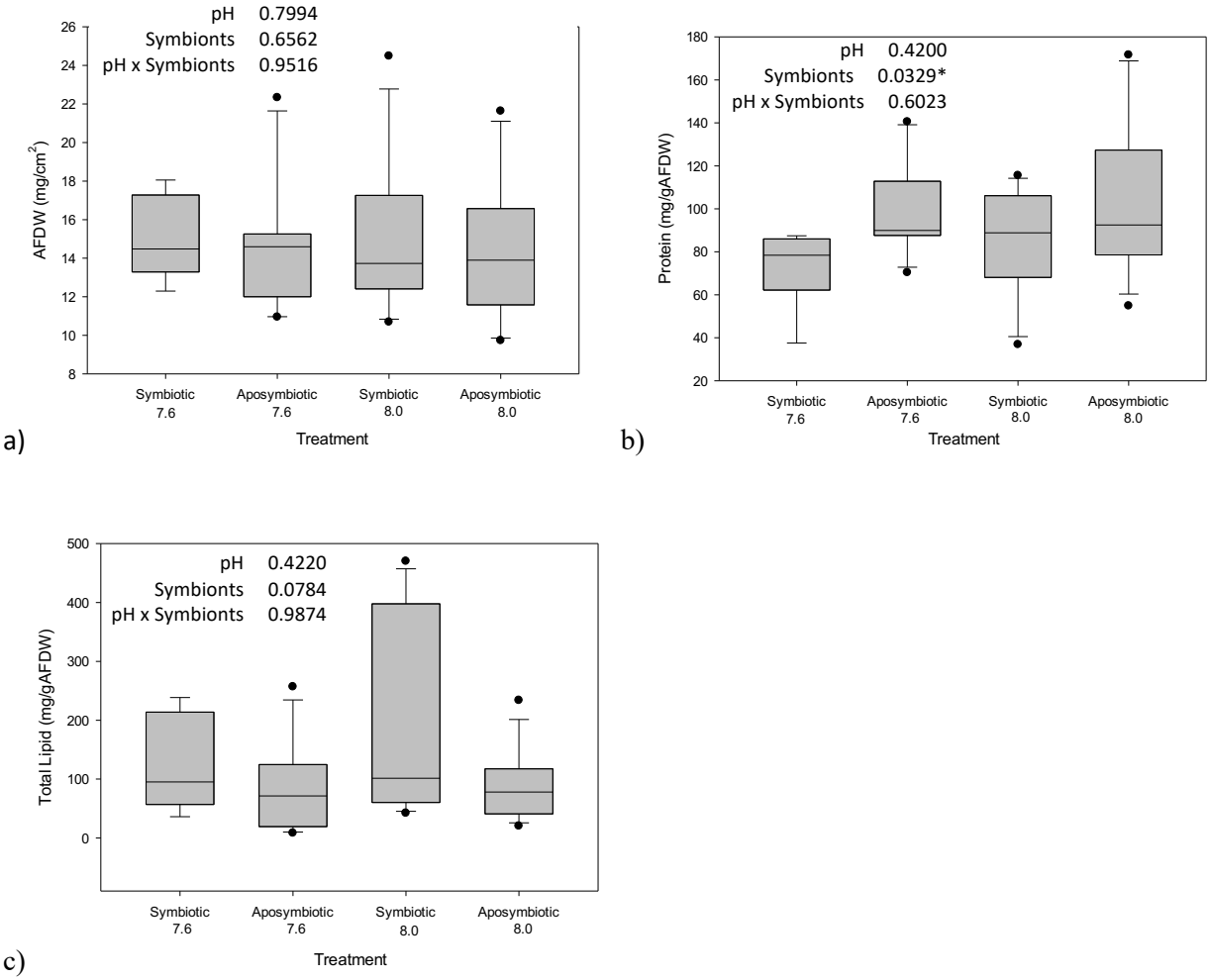

Figure 9. Energetic reserves of symbiotic and aposymbiotic *O. arbuscula* colonies in control pH (8.0) and low pH (7.6) treatments measured as a) AFDW, b) total protein, and c) total lipids. The lower and upper bounds of the boxes indicate the 25th and 75th percentiles, and the extent of the whiskers indicates the 10th and 90th percentiles (n = 12 for symbiotic and aposymbiotic corals at pH 8.0, n=9 for symbiotic corals at pH 7.6 and n=11 for aposymbiotic corals at pH 7.6).

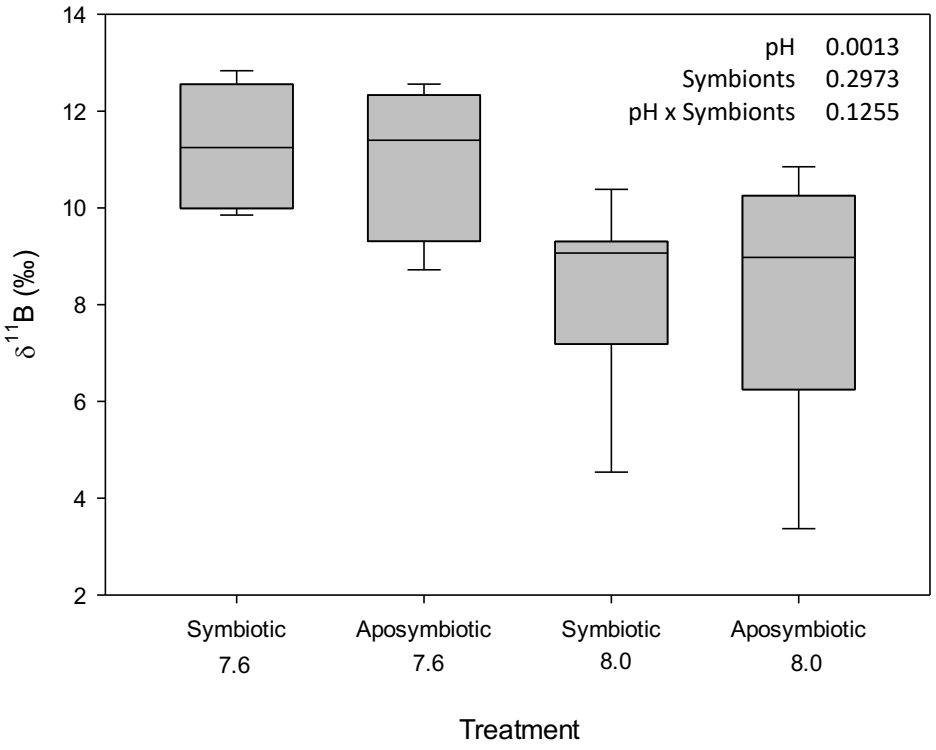

Figure 10. Relative abundance of boron 11 ($\delta^{11}B$) in skeletons of symbiotic and aposymbiotic O. arbuscula colonies in control (8.0) and low pH (7.6) seawater for 51 days. The lower and upper bounds of the boxes indicate the 25th and 75th percentiles, and the extent of the whiskers indicates the 10th and 90th percentiles (n=7 for all conditions except symbiotic corals at pH 7.6 where n=5).

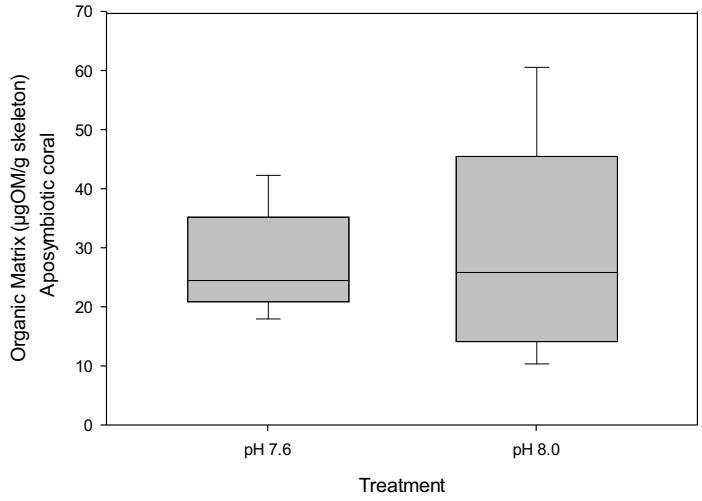

a)

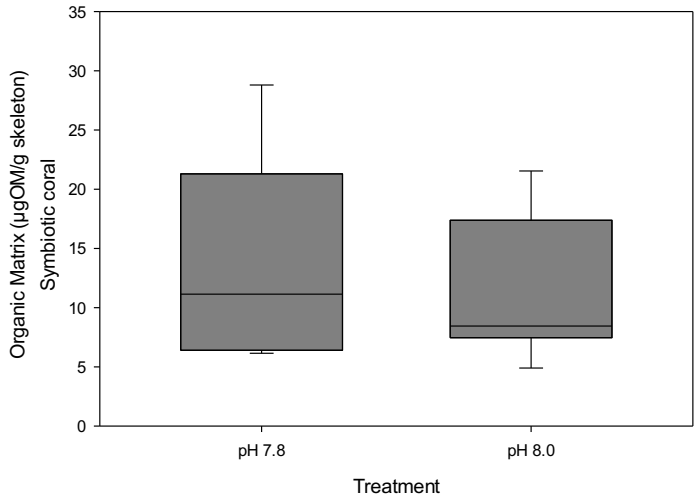

b)

Figure 11. Proteinaceous organic matrix was quantified in *O. arbuscula* colonies from two separate experiments. The present study exposed aposymbiotic coral colonies (a) to control (8.0) and low pH (7.6) for 51 days while Wang et al. (2020) exposed symbiotic coral colonies (b) to control (8.0) and low pH (7.8) for 49 days. The lower and upper bounds of the boxes indicate the 25th and 75th percentiles of the data, and the extent of the whiskers indicates the 10th and 90th percentiles (n =6 and 7 for aposymbiotic and symbiotic colonies, respectively).

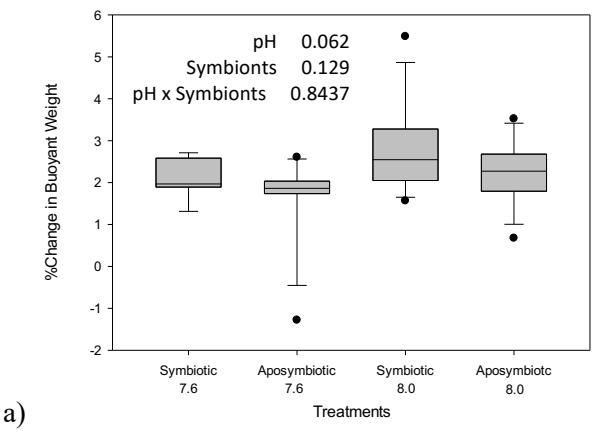

a)

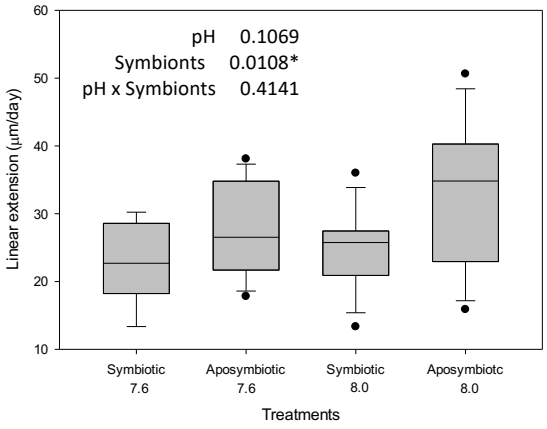

b)

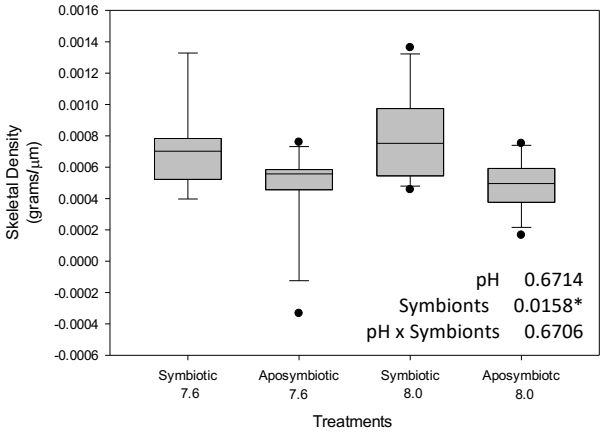

c)

Figure 12. Skeletal growth rate and density in symbiotic and aposymbiotic colonies of *O. arbuscula* exposed to low (7.6) or control (8.0) pH for 51 days. Growth was measured as percent change in buoyant weights (a), linear skeletal extension above the initial alizarin red stain (b), and skeletal density (c). The lower and upper bounds of the boxes indicate the 25th and 75th percentiles and the extent of the whiskers indicate the 10th and 90th percentiles (n = 12 for all treatments except symbiotic corals at low pH where n=9).

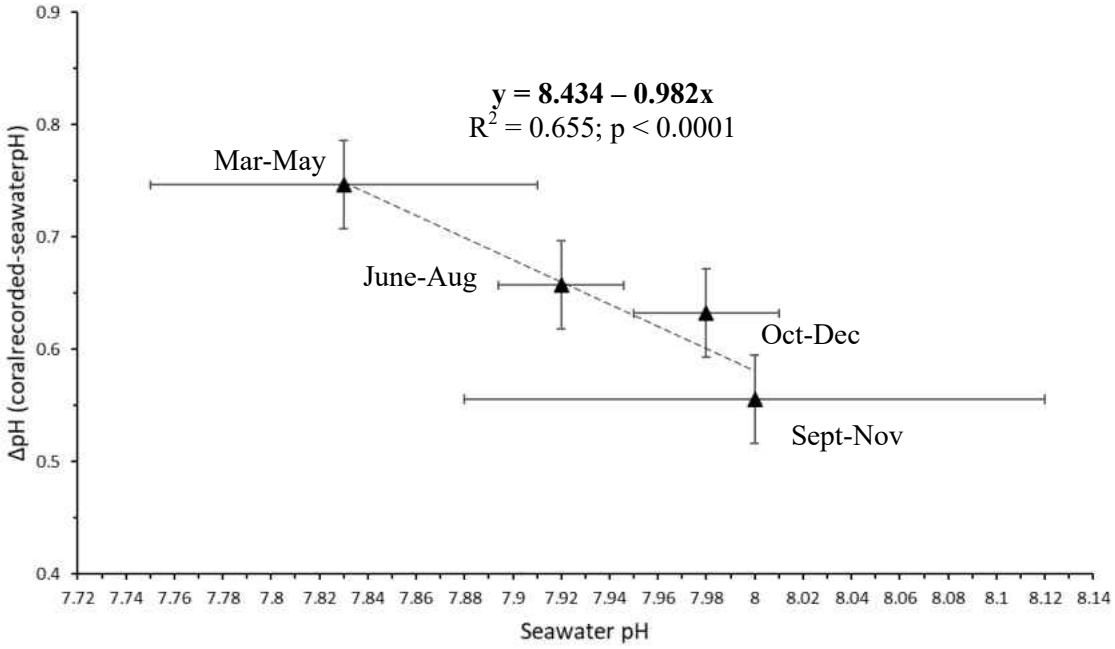

Figure 13. Linear regression showing the relationship between seawater pH and upregulation of calcifying fluid pH (ΔpH) by *O. arbuscula in situ* at GRNMS. Error bars represent standard deviations (n=6 for June-Aug and March-May, n=5 Oct-Dec and Sept-Nov).

CHAPTER 4

DISCUSSION

Seawater pH continues to decrease in the global ocean as CO_2 is emitted into the atmosphere from fossil fuel emissions and is absorbed by seawater. OA reduces the concentration of CO_3^{2-} in seawater, which is potentially detrimental to coral calcification (Egleston et al. 2010). There is significant variability in the impact OA has on calcification rates across coral species (Chan and Connolly 2013; Bove et al. 2019). Resilience demonstrated by some species likely relies on the ability of the coral to handle the energetic costs of maintaining calcifying fluid chemistry and organic matrix production (Figure 3; Cohen and Holcomb 2009). While the algal symbionts present in most scleractinian corals may play a significant role in meeting these energetic demands, partitioning the physiological responses of the coral host versus the symbiotic algae can be difficult because of the obligate nature of this relationship. In this study, I tested the hypothesis that algal symbionts facilitate the acclimatization of corals to OA by focusing on *O. arbuscula*, a temperate scleractinian that exhibits a facultative relationship with symbiotic algae (Figure 3).

My results demonstrated that the resilience of *O. arbuscula* to OA is independent of their symbiotic relationship with the dinoflagellate *B. psygmophilum.* The ability for *O. arbuscula* to maintain calcification rates under reduced seawater pH is driven by control over their calcifying fluid chemistry in both symbiotic and aposymbiotic colonies. Although this process requires additional ATP, *O. arbuscula* is able to meet the energetic demands with or without photosynthetic endosymbionts and also without significantly depleting energy reserves such as lipids and proteins (Figure 14). I infer that *O. arbuscula* relies on heterotrophy for the majority of their energetic needs, questioning the advantage of maintaining a symbiotic relationship with their dinoflagellates. These results suggest the physiology of *O. arbuscula* differs markedly from their tropical counter parts and may not offer an appropriate model for studying OA responses across coral species.

All coral species must biologically control the process of calcification because the initial step of $CaCO_3$ crystal nucleation for biomineralization is kinetically unfavorable (Ridgwell and Zeebe 2005).

Corals facilitate calcification by producing a proteinaceous organic matrix, thus reducing the kinetic energy needed for Ca and CO_3^{2-} to nucleate, and by upregulating their calcifying fluid pH relative to their surrounding seawater ($\Delta pH=pH_{coral}-pH_{seawater}$) (Cohen and McConnaughey 2003; Venn et al. 2011). In the present study, there was no evidence of *O. arbuscula* altering organic matrix production to support calcification rates as seawater pH declined. Instead, by using $\delta^{11}B$ as a relative benchmark, I found that *O. arbuscula* maintained calcifying fluid pH within a specific range. During exposure to low pH in the laboratory, both symbiotic and aposymbiotic *O. arbuscula* colonies maintained skeletal $\delta^{11}B$ at 1.5 ‰ above control pH conditions, a result indicative of higher calcifying fluid pH.

This physiological response observed under controlled conditions in the laboratory was mirrored in *O. arbuscula* colonies grown offshore. Using the boron stable isotope pH proxy for natural seawater, calcifying fluid pH was calculated in corals growing adjacent to a benthic pCO_2 monitoring platform at GRNMS. *Oculina arbuscula* maintained consistent calcifying fluid pH by responding with an equal and opposite ΔpH as seawater pH declined (slope= ~1; Figure 13) even though densities of symbiotic algae fluctuated throughout the year. My boron isotope results obtained for *O. arbuscula* monitored *in situ* agrees with the linear relationship identified in a previous laboratory study using only symbiotic colonies of this species (Figure 15; Liu et al. 2020). Upregulation of calcifying fluid pH as a mechanism imparting OA resilience in *O. arbuscula* appears to be robust, as evidenced by the consistent calcification rates measured in several laboratory studies of both adult and juvenile corals of this species (Ries et al. 2010; Varnerin et al. 2020; Wang et al. 2020). Only when *O. arbuscula* is subjected to OA along with projected increasing temperatures, do their coping mechanisms become overwhelmed. A multi-stressor experiment exposing *O. arbuscula* to a pH of 7.6 crossed with a temperature of 30°C found a tipping point for this coral (Rogers 2019). Calcification rates measured by buoyant weight were significantly reduced when high temperatures and low pH were present, even though single stressor treatments did not cause similar declines in calcification rates (Rogers 2019). I predict that the energetic expenditure required to cope with

temperature or OA individually are manageable in *O. arbuscula,* but the synergistic or additive effects of these stressors exceed the acclimatory capabilities of this coral.

Aichelman et al. (2016) found heterotrophy contributes to the ability of *O. arbuscula* to acclimate to ocean warming and the present study offered insight into the sources of energy available to *O. arbuscula* in regard to coping with OA. In the current study, available energy reserves did not vary with seawater pH (Figure 14). Therefore, the source of ATP for *O. arbuscula* to exert control over the calcifying fluid pH was not sourced from lipid or protein reserves or photosynthetic activities of the symbionts. Presently, the energetic contribution that the symbiotic algae make to the survival and resilience of *O. arbuscula* is unclear. There were differences identified in the energy reserves and calcification between symbiotic an aposymbiotic colonies, but these were not driven by OA. Symbiotic colonies had 2 times greater total lipid content, which can be expected since photosynthetic byproducts are often translocated and stored as lipids (Kellogg and Patton 1983). Contrastingly, aposymbiotic colonies had 1.2 times more protein. This disparity was puzzling because protein is sourced mainly from heterotrophy (Sogin et al. 2016; Schoepf et al. 2017) and all colonies were fed approximately the same concentration of *Artemia spp.* nauplii, ad libitum, twice a week. Since the proliferation of algae is often nitrogen limited, protein or associated compounds may be diverted from prey to symbiotic algae (Piniak et al. 2003; Conlan et al. 2018a). Symbiotic algae can assimilate ~14–23% of the nitrogen obtained from heterotrophy and in the species *Astrangia poculata* more organic nitrogen is excreted from symbiotic than aposymbiotic corals (Szmant-Froelich and Pilson 1984; Piniak et al. 2003; Krueger et al. 2018). High protein levels are also indicative of actively growing sites (Conlan et al. 2018b). Aposymbiotic colonies of *O. arbuscula* exhibited faster linear extension rates, offering another possible explanation for greater protein concentrations found within their tissues.

The additional lipid stores offered by symbionts did not influence calcifying fluid pH upregulation, inciting the question, what is the evolutionarily advantage of maintaining a symbiosis in this facultatively symbiotic coral species? Symbiotic corals had slower linear extension rates but formed

denser skeletons than aposymbiotic colonies. It is possible algal symbionts allow for stronger, denser skeletons resistant to damage by storm surge, physical abrasion, or boring organisms. On the other hand, sacrificing skeletal density for linear extension could be beneficial when growing in a quickly colonized benthic environment where *O. arbuscula* must compete against sponges, tunicates, and other invertebrates for space (ONMS 2012). The growth patterns of *Oculina varicosa* from Florida U.S. may offer insight into our understanding of *O. arbuscula*. *Oculina varicosa* occurs in a range of environments from 6 m depth on Florida coral reefs where colonies are symbiotic, to 80 m deep banks composed of thickets of aposymbiotic colonies. *Oculina varicosa* colonies in shallow waters have slower linear extension rates than aposymbiotic colonies in deep waters suggesting environmental factors may drive a difference in growth patterns (Reed 1982). When symbiotic *O. varicosa* colonies were transplanted to deep water where physical stressors of current, tides and turbidity were reduced, their skeletal growth rates increased but did not equal the rates of the deep water aposymbiotic coral (Reed 1982). This result suggests that both genetic and environmental factors may play a role in controlling calcification rates in this species. In the present study, the aposymbiotic *O. arbuscula* corals that were collected from the inside and outside walls of a shipwreck, sheltered from strong currents, had long branches, and were easily broken. In contrast, the symbiotic corals collected from the top of the ship, exposed to greater physical stress of currents, had shorter branches that were much tougher to remove when sampling. While it is tempting to speculate on the underlying causes of these differences, both genetic polymorphism and phenotypic plasticity are possible explanations and require further investigation.

While there do appear to be potential advantages, in terms of lipid reserves and skeletal density, afforded to *O. arbuscula* by hosting symbiotic algae, there is less interdependency among symbiotic partners than occurs in most tropical coral species. The physiology of this facultatively symbiotic coral seems to be much different than the obligate symbiosis common in tropical corals as evidenced by the ability of *O. arbuscula* to more fully buffer the calcifying fluid pH from the conditions in the surrounding water (Figure 15; Hönisch et al. 2004; Krief et al. 2010; Trotter et al. 2011; Liu et al. 2020). Since many

tropical species studied are unable to maintain their calcifying fluid at a constant pH, they may depend on other mechanisms, such as control of organic matrix production, to maintain higher calcification rates (Lin et al. 2018; Coronado et al. 2019; Glazier et al. 2020). For example, the tropical coral *S. pistillata* exhibits a trend for greater proteinaceous organic matrix when seawater pH decreases (Tambutté et al. 2015). Some researchers even suggest organic matrix may be more critical in the calcification process than calcifying fluid pH in tropical species, by catalyzing the formation of amorphous crystal structures (Falini et al. 2013, 2015; Mass et al. 2013; Lin et al. 2018). The energy used for these calcification processes is primarily sourced from photosynthesis of symbiotic algae in tropical corals.

To avoid introducing another variable into this experiment, heterotrophy was held constant by feeding all colonies twice a week. Corals were allowed to feed to satiation so the concentration of food offered may have been sufficient to offset the energetic requirements to cope with low pH, regardless of their symbiotic status. Several studies corroborate the potential for heterotrophy to offset the energetic costs of calcification to corals exposed to OA (Edmunds 2011; Comeau et al. 2013; Drenkard et al. 2013; Towle et al. 2015). *Oculina arbuscula* has vast opportunities for heterotrophy in the productive waters of the South Atlantic Bight where nutrient rich copepods make up the majority of the zooplankton assemblages (Lopez-Figueroa 2017). Enriched *Artemia spp.* nauplii were fed to the corals in this experiment, which can be equally or less nutrient dense as natural samples of zooplankton (Helland et al. 2003; van der Meeren et al. 2008; Conlan et al. 2018a). *Artemia* nauplii are often enriched in lipids, but copepods often offer higher concentrations of fatty acids as an important source of metabolic energy in the form of ATP (Helland et al. 2003; van der Meeren et al. 2008; Conlan et al. 2018a). *Oculina arbuscula* also consumes prey as small as pico- and nanoplankton (< 10 μm) offshore (Piniak 2002; Leal et al. 2014). The potential contribution of pico- and nanoplankton is not trivial, constituting an important food source in both symbiotic and aposymbiotic coral species potentially supplying 52-82% of nitrogen ingested (Houlbreque et al 2004). Therefore, I do not believe the feeding regime and nutrients offered during my study skewed the response to OA from what would be seen offshore by *O. arbuscula*. The

abundance of prey available and versatility of items consumed suggest the diet of *O. arbuscula* will likely offer sufficient energy for this species to be successful in changing seawater chemistry, provided the abundance of nutrient rich prey such as copepods are not also impacted by OA (Hatcher 1990; Verity et al. 1993; Dave and Lozier 2013; Cripps et al. 2014).

The results of my laboratory experiment, supported by my *in situ* study demonstrating the relationship between ΔpH and seawater pH offshore, emphasize the importance of control over calcifying fluid pH for the success of *O. arbuscula* off the coast of the southeastern U.S.A. These results provide significant insight into the mechanisms behind *O. arbuscula*'s resilience to OA (Ries et al. 2010; Varnerin et al. 2020; Wang et al. 2020). I conclude that natural variations in pCO_2 have, over evolutionary time, resulted in a coral species well-adapted to cope with significant environmental swings in pH. In addition, inconsistent light availability in their range has reduced dependence on symbiotic algae in *O. arbuscula* so algal presence does not dictate the resilience of this species to OA conditions. *Oculina arbuscula* is likely to have greater success in future seawater pH conditions than other coral species, hopefully continuing to contribute to the structural complexity of live bottom reef habitats such as GRNMS.

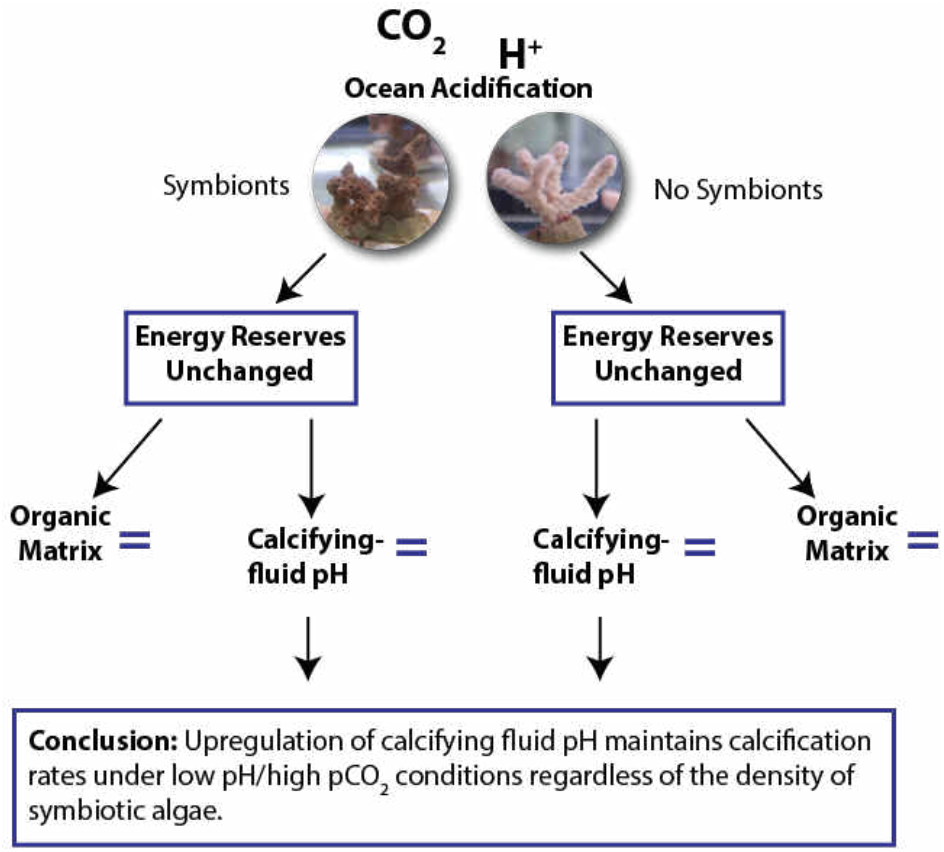

Figure 14. Flow chart following the results from the experimental trial testing the role of symbiotic algae in the acclimatization response of *O. arbuscula* to OA. An equal sign denotes that the response for the variable of interest, production of organic matrix or alteration of calcifying fluid pH, was similar for corals maintained under control (8.0) and low (7.6) pH conditions for 51 days.

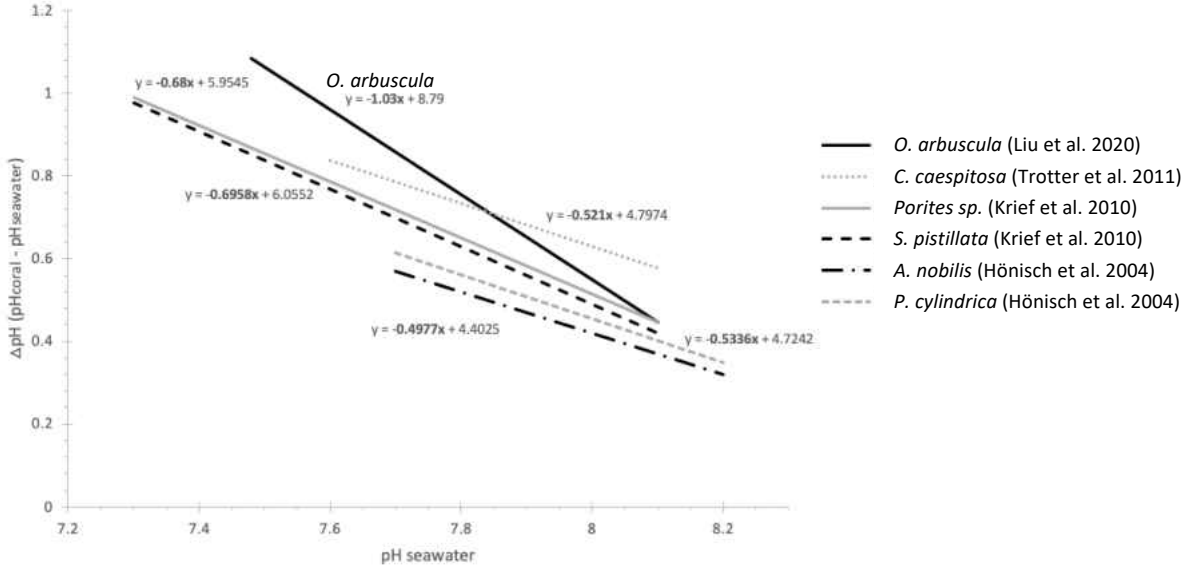

Figure 15. Regressions found for the temperate coral species *O. arbuscula* (Liu et al. 2020) and *C. caespitosa* (Trotter et al. 2011) and the tropical corals *Porites sp., Acropora noblis, and Stylophora pistillata* (Hönisch et al. 2004; Krief et al. 2010) that define the relationship between calcifying fluid ($\Delta pH = pH_{calcifying\ fluid} - pH_{seawater}$) and seawater pH. The ability to increase ΔpH differs between species, which is defined by the slope in this graph.

REFERENCES

Adamiano, A., S. Goffredo, Z. Dubinsky, O. Levy, S. Fermani, and D. Fabbri. 2014. Analytical pyrolysis-based study on intra-skeletal organic matrices from Mediterranean corals. Anal. Bioanal. Chem. 406: 6021–6033.

Al-Horani, F. A., S. M. Al-Moghrabi, and D. De Beer. 2003. Microsensor study of photosynthesis and calcification in the scleractinian coral, *Galaxea fascicularis*: Active internal carbon cycle. J. Exp. Mar. Bio. Ecol. 288: 1–15.

Allemand, D., C. Ferrier-pagès, P. Furla, F. Houlbrèque, and C. Darwin. 2004. Biomineralisation in reef-building corals: from molecular mechanisms to environmental control. Palaeobiochemistry. 3: 453–467.

Allemand D., É. Tambutté, D. Zoccola, S. Tambutté. (2011) Coral Calcification, Cells to Reefs. In: Dubinsky Z., Stambler N. (eds) Coral Reefs: An Ecosystem in Transition. Springer, Dordrecht. https://doi.org/10.1007/978-94-007-0114-4_9

Anagnostou, E., K. F. Huang, C. F. You, E. L. Sikes, and R. M. Sherrell. 2012. Evaluation of boron isotope ratio as a pH proxy in the deep sea coral *Desmophyllum dianthus*: Evidence of physiological pH adjustment. Earth Planet. Sci. Lett. 349–350: 251–260.

Bauer, J. E., W. J. Cai, P. A. Raymond, T. S. Bianchi, C. S. Hopkinson, and P. A. G. Regnier. 2013. The changing carbon cycle of the coastal ocean. Nature. 504: 61–70.

Bertucci, A., A. Moya, S. Tambutté, D. Allemand, C. T. Supuran, and D. Zoccola. 2013. Carbonic anhydrases in anthozoan corals - A review. Bioorganic Med. Chem. 21: 1437–1450.

Bindoff, N.L., W.W.L. Cheung, J.G. Kairo, J. Arístegui, V.A. Guinder, R. Hallberg, N. Hilmi, N. Jiao, M.S. Karim, L. Levin, S. O'Donoghue, S.R. Purca Cuicapusa, B. Rinkevich, T. Suga, A. Tagliabue, and P. Williamson, 2019: Changing Ocean, Marine Ecosystems, and Dependent Communities. In:

IPCC Special Report on the Ocean and Cryosphere in a Changing Climate [H.-O. Pörtner, D.C. Roberts, V. Masson-Delmotte, P. Zhai, M. Tignor, E. Poloczanska, K. Mintenbeck, A. Alegría, M. Nicolai, A. Okem, J. Petzold, B. Rama, N.M. Weyer (eds.)]. In press. 477-587.

Bove, C. B., J. B. Ries, S. W. Davies, I. T. Westfield, J. Umbanhowar, and K. D. Castillo. 2019. Common Caribbean corals exhibit highly variable responses to future acidification and warming. Proc. R. Soc. B Biol. Sci. 286(2840): 1-9.

Burke, L., Reytar, K., Spalding, M., & Perry, A. 2011. Reefs at risk revisited. World Resources Institute. Washington, D.C. 11-14.

Chan, N. C. S., and S. R. Connolly. 2013. Sensitivity of coral calcification to ocean acidification: A meta-analysis. Glob. Chang. Biol. 19: 282–290.

Cohen, A., and M. Holcomb. 2009. Why corals care about ocean acidification: Uncovering the mechanism. Oceanography. 22: 118–127.

Cohen, A. L., and T. A. McConnaughey. 2003. Geochemical perspectives on coral mineralization. Rev. Mineral Geochemistry. 54: 151–187.

Comeau, S., R. C. Carpenter, and P. J. Edmunds. 2013. Effects of feeding and light intensity on the response of the coral *Porites rus* to ocean acidification. Mar. Biol. 160: 1127–1134.

Comeau, S., P. J. Edmunds, N. B. Spindel, and R. C. Carpenter. 2014. Fast coral reef calcifiers are more sensitive to ocean acidification in short-term laboratory incubations. Limnol. Oceanogr. 59: 1081–1091.

Conlan, J. A., L. K. Bay, A. Severati, C. Humphrey, and D. S. Francis. 2018a. Comparing the capacity of five different dietary treatments to optimise growth and nutritional composition in two scleractinian corals. PLoS One. 13: 1–20.

Conlan, J. A., C. A. Humphrey, A. Severati, and D. S. Francis. 2018b. Intra-colonial diversity in the

scleractinian coral, *Acropora millepora*: Identifying the nutritional gradients underlying physiological integration and compartmentalised functioning. PeerJ. 6(4239): 1-20.

Coronado, I., M. Fine, F. R. Bosellini, and J. Stolarski. 2019. Impact of ocean acidification on crystallographic vital effect of the coral skeleton. Nat. Commun. 10(2896): 1-9.

Cripps, G., P. Lindeque, and K. J. Flynn. 2014. Have we been underestimating the effects of ocean acidification in zooplankton? Glob. Chang. Biol. 20: 3377–3385.

Dauphin, Y., J.-P. Cuif, and P. Massard. 2006. Persistent organic components in heated coral aragonitic skeletons--Implications for palaeoenvironmental reconstructions. Chem. Geol. 231: 26–37.

Dave, A. C., and M. S. Lozier. 2013. Examining the global record of interannual variability in stratification and marine productivity in the low-latitude and mid-latitude ocean. J. Geophys. Res. Ocean. 118: 3114–3127.

Davies, P. S. 1989. Short-term growth measurements of corals using an accurate buoyant weighing technique. Mar. Biol. 101: 389–395.

Dickson, A. 1990. Thermodynamics of the dissociation of boric-acid in synthetic seawater from 273.15-K to 318.15-K. Deep Sea Res. Part I Oceanogr. Res. Pap. 37: 755–766.

Dickson, A. G. 2011. The carbon dioxide system in seawater: equilibrium chemistry and measurements. In: Guide to best practices for ocean acidification research and data reporting. Office for Official Publications of the European Communities. Luxembourg, Belgium. 17-40.

Dissard, D., E. Douville, S. Reynaud, P. Montagna, P. Louvat, M. Mcculloch, and A. Saint-martin. 2012. Light and temperature effects on $\delta^{11}B$ and B/Ca ratios of the zooxanthellate coral *Acropora sp.*: results from culturing experiments. Biogeosciences. 9: 4589–4605.

Doney, S. C., V. J. Fabry, R. A. Feely, and J. A. Kleypas. 2009. Ocean Acidification: The other CO_2 problem. Ann. Rev. Mar. Sci. 1: 169–192.

Drake, J. L., T. Mass, L. Haramaty, E. Zelzion, D. Bhattacharya, and P. G. Falkowski. 2013. Proteomic analysis of skeletal organic matrix from the stony coral *Stylophora pistillata.* PNAS. 110: 3788–3793.

Drenkard, E. J., A. L. Cohen, D. C. McCorkle, S. J. de Putron, V. R. Starczak, and A. E. Zicht. 2013. Calcification by juvenile corals under heterotrophy and elevated CO_2. Coral Reefs. 32: 727–735.

Edmunds, P. J. 2011. Zooplanktivory ameliorates the effects of ocean acidification on the reef coral *Porites spp*. Limnol. Oceanogr. 56: 2402–2410.

Edmunds, P. J., S. Comeau, C. Lantz, A. Andersson, C. Briggs, A. Cohen, J. Gattuso, J.M. Grady, K. Gross, M. Johnson, E.B. Muller, J.B. Ries, S. Tambutté, E. Tambutté, A. Venn, and R. Carpenter. 2016. Integrating the effects of ocean acidification across functional scales on tropical toral reefs. Bioscience. 66: 350–362.

Edmunds, P. J., and R. D. Gates. 2002. Normalizing physiological data for scleractinian corals. Coral Reefs. 21: 193–197.

Egleston, E. S., C. L. Sabine, and F. M. M. Morel. 2010. Revelle revisited: Buffer factors that quantify the response of ocean chemistry to changes in DIC and alkalinity. Global Biogeochem. Cycles. 24: 1–9.

Von Euw, S., Q. Zhang, V. Manichev, N. Murali, J. Gross, L.C. Feldman, T. Gustafsson, C. Flach, R. Mendelsohn, P.G. Falkowski. 2017. Biological control of aragonite formation in stony corals. Science. 356: 933–938.

Fabricius, K. E., G. De, S. Noonan, and S. Uthicke. 2014. Ecological effects of ocean acidification and habitat complexity on reef-associated macroinvertebrate communities. Proc. R. Soc. B Biol. Sci. 281: 20132479 1-8.

Falini, G., S. Fermani, and S. Goffredo. 2015. Coral biomineralization: A focus on intra-skeletal organic

matrix and calcification. Semin. Cell Dev. Biol. 46: 17–26.

Falini, G., M. Reggi, S. Fermani, F. Sparla, S. Goffredo, Z. Dubinsky, O. Levi, Y. Dauphin, and J. Cuif. 2013. Control of aragonite deposition in colonial corals by intra-skeletal macromolecules. J. Struct. Biol. 183: 226–238.

Foster, G. L. 2008. Seawater pH, pCO_2 and $[CO_3^{2-}]$ variations in the Caribbean Sea over the last 130 kyr: A boron isotope and B/Ca study of planktic foraminifera. Earth Planet. Sci. Lett. 271: 254–266.

Gaillardet, J., D. Lemarchand, C. Göpel, and G. Manhès. 2001. Evaporation and sublimation of boric acid: Application for boron purification from organic rich solutions. Geostand. Newsl. 25: 67–75.

Glazier, A., S. Herrera, A. Weinnig, M. Kurman, C. E. Gómez, and E. Cordes. 2020. Regulation of ion transport and energy metabolism enables certain coral genotypes to maintain calcification under experimental ocean acidification. Mol. Ecol. 29: 1657–1673.

Gleason, D. F., L. R. Harbin, L. M. Divine, and K. O. Matterson. 2018. The role of larval supply and competition in controlling recruitment of the temperate coral *Oculina arbuscula.* J. Exp. Mar. Bio. Ecol. 506: 107–114.

Goldberg, W. M. 2001. Acid polysaccharides in the skeletal matrix and calicoblastic epithelium of the stony coral *Mycetophyllia reesi*. Tissue Cell. 33: 376–387.

Gori, A., C. Ferrier-pagès, S. J. Hennige, F. Murray, C. Rottier, L. C. Wicks, and J. M. Roberts. 2016. Physiological response of the cold-water coral *Desmophyllum dianthus* to thermal stress and ocean acidification. PeerJ. 4(1606): 1-16.

Griffiths, J. S., T. C. F. Pan, and M. W. Kelly. 2019. Differential responses to ocean acidification between populations of *Balanophyllia elegans* corals from high and low upwelling environments. Mol. Ecol. 28: 2715–2730.

Grottoli-Everett, A. G., and I. B. Kuffner. 1995. Uneven bleaching within colonies of the Hawaiian coral

Montipora verrucosa. Ultraviolet Radiation and Coral Reefs. 41: 115–120.

Grottoli, A. G., L. J. Rodrigues, and C. Juarez. 2004. Lipids and stable carbon isotopes in two species of Hawaiian corals, *Porites compressa* and *Montipora verrucosa,* following a bleaching event. Mar. Biol. 145: 621–631.

Hatcher, B. G. 1990. Coral reef primary productivity: A hierarchy of pattern and process. Trends Ecol. Evol. 5: 149–155.

Helland, S., B. F. Terjesen, and L. Berg. 2003. Free amino acid and protein content in the planktonic copepod *Temora longicornis* compared to *Artemia franciscana*. Aquaculture. 215: 213–228.

Hennige, S. J., L. C. Wicks, N. A. Kamenos, D. C. E. Bakker, H. S. Findlay, C. Dumousseaud, and J. M. Roberts. 2014. Short-term metabolic and growth responses of the cold-water coral *Lophelia pertusa* to ocean acidification. Deep Sea Res. Part II Top. Stud. Oceanogr. 99: 27–35.

Holcomb, M., A. A. Venn, E. Tambutté, S. Tambutté, D. Allemand, J. Trotter, and M. McCulloch. 2014. Coral calcifying fluid pH dictates response to ocean acidification. Sci. Rep. 4(5207): 1-4.

Hönisch, B., Ng. Hemming, A. G. Grottoli, A. Amat, G. N. Hanson, and J. Bijma. 2004. Assessing scleractinian corals as recorders for paleo-pH: Empirical calibration and vital effects. Geochim. Cosmochim. Acta. 68: 3675–3685.

Hopkinson, B. M., A. L. Tansik, and W. K. Fitt. 2015. Internal carbonic anhydrase activity in the tissue of scleractinian corals is sufficient to support proposed roles in photosynthesis and calcification. J. Exp. Biol. 218: 2039–2048.

Huang, D., E. E. Goldberg, L. M. Chou, and K. Roy. 2018. The origin and evolution of coral species richness in a marine biodiversity hotspot. Evolution. 72: 288–302.

Jeffrey, S. W., and G. F. Humphrey. 1975. New spectrophotometric equations for determining chlorophylls a, b, c1 and c2 in higher plants, algae and natural phytoplankton. Biochem. Physiol.

Pflanz. 167: 191–194.

Kellogg, R. B., and J. S. Patton. 1983. Lipid droplets, medium of energy exchange in the symbiotic anemone *Condylactis gigantea*: a model coral polyp. Mar. Biol. 75: 137–149.

Klochko, K., A. J. Kaufman, W. Yao, R. H. Byrne, and J. A. Tossell. 2006. Experimental measurement of boron isotope fractionation in seawater. Earth Planet. Sci. Lett. 248: 261–270.

Krief, S., E. J. Hendy, M. Fine, R. Yam, A. Meibom, G. L. Foster, and A. Shemesh. 2010. Physiological and isotopic responses of scleractinian corals to ocean acidification. Geochim. Cosmochim. Acta. 74: 4988–5001.

Kroeker, K. J., R. L. Kordas, R. Crim, I. E. Hendriks, L. Ramajo, G. S. Singh, C. M. Duarte, and J. P. Gattuso. 2013. Impacts of ocean acidification on marine organisms: Quantifying sensitivities and interaction with warming. Glob. Chang. Biol. 19: 1884–1896.

Krueger, T., J. Bodin, N. Horwitz, C. Loussert-Fonta, A. Sakr, S. Escrig, M. Fine, and A. Meibom. 2018. Temperature and feeding induce tissue level changes in autotrophic and heterotrophic nutrient allocation in the coral symbiosis – A NanoSIMS study. Sci. Rep. 8: 1–15.

Lamberts, A. E. 1973. Alizarin deposition by corals. [Dissertation] University of Hawaii. Honolulu, HI. 1-114.

Leal, M. C., C. Ferrier-Pages, R. Calado, J. A. Brandes, M. E. Frischer, and J. C. Nejstgaard. 2014. Trophic ecology of the facultative symbiotic coral *Oculina arbuscula*. Mar. Ecol. Prog. Ser. 504: 171–179.

Lin, Z., L. Wang, M. Chen, and J. Chen. 2018. The acute transcriptomic response of coral-algae interactions to pH fluctuation. Mar. Genomics. 42: 32–40.

Liu, Y. W., J. N. Sutton, J. B. Ries, and R. A. Eagle. 2020. Regulation of calcification site pH is a polyphyletic but not always governing response to ocean acidification. Sci. Adv. 6: 1–8.

Maier, C., P. Popp, N. Sollfrank, M. G. Weinbauer, C. Wild, and J.-P. Gattuso. 2016. Effects of elevated pCO_2 and feeding on net calcification and energy budget of the Mediterranean cold-water coral *Madrepora oculata*. J. Exp. Biol. 219: 3208–3217.

Marubini, F., C. Ferrier-Pages, and J.-P. Cuif. 2003. Suppression of skeletal growth in scleractinian corals by decreasing ambient carbonate-ion concentration: a cross-family comparison. Proc. R. Soc. B Biol. Sci. 270: 179–184.

Mass, T., J. L. Drake, L. Haramaty, J. D. Kim, E. Zelzion, D. Bhattacharya, and P. G. Falkowski. 2013. Cloning and characterization of four novel coral acid-rich proteins that precipitate carbonates *in vitro*. Curr. Biol. 23: 1126–1131.

McCulloch, M., J. Trotter, P. Montagna, J. Falter, R. Dunbar, A. Freiwald, G. Försterra, M. L. Correa, C. Maier, A. Rüggeberg, and M. Taviani. 2012. Resilience of cold-water scleractinian corals to ocean acidification: Boron isotopic systematics of pH and saturation state up-regulation. Geochim. Cosmochim. Acta. 87: 21–34.

van der Meeren, T., R. E. Olsen, K. Hamre, and H. J. Fyhn. 2008. Biochemical composition of copepods for evaluation of feed quality in production of juvenile marine fish. Aquaculture. 274: 375–397.

Movilla, J., E. Calvo, R. Coma, E. Serrano, and À. López. 2016. Annual response of two Mediterranean azooxanthellate temperate corals to low - pH and high - temperature conditions. Mar. Biol. 163: 1–14.

Muscatine, L., P. Falkowski, J. Porter, and Z. Dubinsky. 1984. Primary production and photoadaptation in light- and shade-adapted colonies of the symbiotic coral, *Stylophora pistillata.* Proc. R. Soc. London. Ser. B. Biol. Sci. 222: 161–180.

Noakes S. 2020. Carbon dioxide and water quality monitoring in Gray's Reef National Marine Sanctuary, 2006-2014. In: Roberson KW, Auster PJ, Fangman S, Harvey M (eds) Review of scientific research

in and around the designated research area of Gray's Reef National Marine Sanctuary (NW Atlantic). NOAA, Silver Spring, MD.

Noireaux J, V. Mavromatis, J. Gaillardet, J. Schott, V. Montouillout, P. Louvat, C. Rollion-bard, and D.R. Neuville. 2015. Crystallographic control on the boron isotope paleo-pH proxy. Earth Planet Sci. Lett. 430: 398–407.

Noireaux, J., V. Mavromatis, J. Gaillardet, J. Schott, V. Montouillout, P. Louvat, C. Rollion-bard, and D. R. Neuville. 2015. Crystallographic control on the boron isotope paleo-pH proxy. Earth Planet. Sci. Lett. 430: 398–407.

Office of National Marine Sanctuaries. McFall, G., Sedberry, G., Shortland., B. Gray's Reef National Marine Sanctuary Condition Report Addendum 2012. U.S. Department of Commerce, National Oceanic and Atmospheric Administration. 1-36.

Okazaki, R. R., P. K. Swart, and C. Langdon. 2013. Stress-tolerant corals of Florida Bay are vulnerable to ocean acidification. Coral Reefs. 32: 671–683.

Orr, J.C., V.J. Fabry, O. Aumont, L. Bopp, S.C. Doney, R.A. Feely, A. Gnanadesikan, N. Gruber, A. Ishida, F. Joos, and R.M. Key. 2005. Anthropogenic ocean acidification over the twenty-first century and its impact on calcifying organisms. Nature. 437: 681–686.

Piniak, G.A. 2002. Effects of symbiotic status, flow speed, and prey type on prey capture by the facultatively symbiotic temperate coral *Oculina arbuscula*. Mar. Biol. 141: 449–455.

Piniak, G.A., F. Lipschultz, and J. McClelland. 2003. Assimilation and partitioning of prey nitrogen within two anthozoans and their endosymbiotic zooxanthellae. Mar. Ecol. Prog. Ser. 262: 125–136.

Pörtner, H.O. 2008. Ecosystem effects of ocean acidification in times of ocean warming: A physiologist's view. Mar. Ecol. Prog. Ser. 373: 203–217.

Raybaud, V., S. Tambutté, C. Ferrier-Pagès, S. Reynaud, A. A. Venn, É. Tambutté, P. Nival, and D.

Allemand. 2017. Computing the carbonate chemistry of the coral calcifying medium and its response to ocean acidification. J. Theor. Biol. 424: 26–36.

Reed, J. K. 1982. *In situ* growth rates of the scleractinian coral *Oculina varicosa* occurring with zooxanthellae on 6-m reefs and without on 80-m banks. Proc. 4th Int. Coral Reef Symp. 2: 201–206.

Ridgwell, A., and R. E. Zeebe. 2005. The role of the global carbonate cycle in the regulation and evolution of the Earth system. Earth Planet. Sci. Lett. 234: 299–315.

Ries, J. B., A. L. Cohen, and D. C. McCorkle. 2009. Marine calcifiers exhibit mixed responses to CO_2-induced ocean acidification. Geology. 37: 1131–1134.

Ries, J. B., A. L. Cohen, and D. C. McCorkle. 2010. A nonlinear calcification response to CO_2-induced ocean acidification by the coral *Oculina arbuscula*. Coral Reefs. 29: 661–674.

Rodolfo-Metalpa, R., S. Martin, C. Ferrier-Pages, and J. P. Gattuso. 2010. Response of the temperate coral *Cladocora caespitosa* to mid- and long-term exposure to pCO_2 and temperature levels projected for the year 2100 AD. Biogeosciences. 7: 289–300.

Rodolfo-Metalpa, R., P. Montagna, S. Aliani, M. Borghini, S. Canese, J.M. Hall-Spencer, A. Foggo, M. Milazzo, M. Taviani, and F. Houlbrèque. 2015. Calcification is not the Achilles' heel of cold-water corals in an acidifying ocean. Glob. Chang. Biol. 21: 2238–2248.

Rodrigues, L. J., and A. G. Grottoli. 2006. Calcification rate and the stable carbon, oxygen, and nitrogen isotopes in the skeleton, host tissue, and zooxanthellae of bleached and recovering Hawaiian coral. Geochim. Cosmochim. Acta. 70: 2781–2789.

Rogers, S. 2019. The combined effects of pH and temperature on the physiology of the temperate coral *Oculina arbuscula*. Honors College Theses. 427. https://digitalcommons.georgiasouthern.edu/honors-theses/427

Schoepf, V., C. P. Jury, R. J. Toonen, and M. T. McCulloch. 2017. Coral calcification mechanisms

facilitate adaptive responses to ocean acidification. Proc. R. Soc. B Biol. Sci. 284(1868): 1-9.

Sevilgen, D. S., A. A. Venn, M. Y. Hu, E. Tambutté, D. De Beer, V. Planas-Bielsa, and S. Tambutté. 2019. Full *in vivo* characterization of carbonate chemistry at the site of calcification in corals. Sci. Adv. 5(7447): 1-9.

Smith, P. K., R. I. Krohn, G. T. Hermanson, A.K. Mallia, F.H. Gartner, M. Provenzano, E.K. Fujimoto, N.M. Goeke, B.J. Olson, and D.C. Klenk. 1985. Measurement of protein using bicinchoninic acid. Anal. Biochem. 150: 76–85.

Sogin, E. M., H. M. Putnam, P. E. Anderson, and R. D. Gates. 2016. Metabolomic signatures of increases in temperature and ocean acidification from the reef-building coral, *Pocillopora damicornis*. Metabolomics. 12: 71.

Stewart, J. A., S. J. Christopher, J. R. Kucklick, L. Bordier, T.B. Chalk, A. Dapoigny, E. Douville, G.L. Foster, W.R. Gray, R. Greenop, M. Gutjahr, F. Hemsing, M.J. Henehan, P. Holdship, Y.T. Hsieh, A. Kolevica, Y.P. Lin, E.M. Mawbey, J.W.B. Rae, L.F. Robinson, R. Shuttleworth, C.F. You, S. Zhang, and R.D. Day. 2021. NIST RM 8301 Boron isotopes in marine carbonate (simulated coral and foraminifera solutions): Inter-laboratory $\delta^{11}B$ and trace element ratio value assignment. Geostand. Geoanalytical Res. 45: 77–96.

Szmant-Froelich, A., and M. E. Q. Pilson. 1984. Effects of feeding frequency and symbiosis with zooxanthellae on nitrogen metabolism and respiration of the coral *Astrangia danae*. Mar. Biol. 81: 153–162.

Tambutté, E., A. A. Venn, M. Holcomb, N. Segonds, N. Techer, D. Zoccola, D. Allemand, and S. Tambutté. 2015. Morphological plasticity of the coral skeleton under CO_2-driven seawater acidification. Nat. Commun. 6: 1–9.

Thornhill, D. J., D. W. Kemp, B. U. Bruns, W. K. Fitt, and G. W. Schmidt. 2008. Correspondence

between cold tolerance and temperate biogeography in a western Atlantic Symbiodinium (Dinophyta) lineage. J. Phycol. 44: 1126–1135.

Towle, E. K., I. C. Enochs, and C. Langdon. 2015. Threatened Caribbean coral is able to mitigate the adverse effects of ocean acidification on calcification by increasing feeding rate. PLoS One. 10: 1–18.

Trotter, J., P. Montagna, M. McCulloch, S. Silenzi, S. Reynaud, G. Mortimer, S. Martin, C. Ferrier-Pagès, J.P. Gattuso, and R. Rodolfo-Metalpa. 2011. Quantifying the pH "vital effect" in the temperate zooxanthellate coral *Cladocora caespitosa*: Validation of the boron seawater pH proxy. Earth Planet. Sci. Lett. 303: 163–173.

Varnerin, B. V, B. M. Hopkinson, and D. F. Gleason. 2020. Recruits of the temperate coral *Oculina arbuscula* mimic adults in their resilience to ocean acidification. Mar. Ecol. Prog. Ser. 636: 63–75.

Venn, A., E. Tambutté, M. Holcomb, D. Allemand, and S. Tambutté. 2011. Live tissue imaging shows reef corals elevate pH under their calcifying tissue relative to seawater. PLoS One. 6(20013): 1-9.

Verity, P. G., J. A. Yoder, S. Stephen Bishop, J. R. Nelson, D. B. Craven, J. O. Blanton, C. Y. Robertson, and C. R. Tronzo. 1993. Composition, productivity and nutrient chemistry of a coastal ocean planktonic food web. Cont. Shelf Res. 13: 741–776.

Wall, C. B., R. A. B. Mason, W. R. Ellis, R. Cunning, and R. D. Gates. 2017. Elevated pCO_2 affects tissue biomass composition, but not calcification, in a reef coral under two light regimes. R. Soc. Open Sci. 4: 1–13.

Wang, B. S., C. F. You, K. F. Huang, S. F. Wu, S. K. Aggarwal, C. H. Chung, and P. Y. Lin. 2010. Direct separation of boron from Na- and Ca-rich matrices by sublimation for stable isotope measurement by MC-ICP-MS. Talanta. 82: 1378–1384.

Wang, C., E. M. Arneson, D. F. Gleason, and B. M. Hopkinson. 2020. Resilience of the temperate coral

Oculina arbuscula to ocean acidification extends to the physiological level. Coral Reefs. 40: 201–214.

Wanninkhof, R., L. Barbero, R. Byrne, W. J. Cai, W. J. Huang, J. Z. Zhang, M. Baringer, and C. Langdon. 2015. Ocean acidification along the Gulf Coast and East Coast of the USA. Cont. Shelf Res. 98: 54–71.

Weiner, S., and P. Dove. 2003. An overview of biomineralization processes and the problem of the vital effect. Rev. Mineral Geochemistry. 54: 1–29.

Wood, H. L., J. I. Spicer, and S. Widdicombe. 2008. Ocean acidification may increase calcification rates, but at a cost. Proc. R. Soc. B Biol. Sci. 275: 1767–1773.

Zhang, H., and R. H. Byrne. 1996. Spectrophotometric pH measurements of surface seawater at *in-situ* conditions: Absorbance and protonation behavior of thymol blue. Mar. Chem. 52: 17–25.